HHS Public Access

Author manuscript

Nature. Author manuscript; available in PMC 2015 July 29.

Published in final edited form as:

Nature. 2015 January 29; 517(7536): 626–630. doi:10.1038/nature13910.

IAPP driven metabolic reprogramming induces regression of *p53* - deficient tumours *in vivo*

Avinashnarayan Venkatanarayan[1,2,3,4], **Payal Raulji**[1,2], **William Norton**[5], **Deepavali Chakravarti**[1,2,3,4], **Cristian Coarfa**[9], **Xiaohua Su**[1,2,4], **Santosh K. Sandur**[1,2,4,11], **Marc S. Ramirez**[6], **Jaehuk Lee**[6], **Charles V. Kingsley**[6], **Eliot F. Sananikone**[1,2,3,4], **Kimal Rajapakshe**[9], **Katherine Naff**[5], **Jan Parker-Thornburg**[8], **James A. Bankson**[6], **Kenneth Y. Tsai**[2,7], **Preethi H. Gunaratne**[10], and **Elsa R. Flores**[1,2,3,4,12]

[1]Department of Molecular and Cellular Oncology, The University of Texas M.D. Anderson Cancer Center, 1515 Holcombe Blvd., Houston, TX 77030, USA

[2]Department of Translational Molecular Pathology, The University of Texas M.D. Anderson Cancer Center, 1515 Holcombe Blvd., Houston, TX 77030, USA

[3]Graduate School of Biomedical Sciences, The University of Texas M.D. Anderson Cancer Center, 1515 Holcombe Blvd., Houston, TX 77030, USA

[4]Metastasis Research Center, The University of Texas M.D. Anderson Cancer Center, 1515 Holcombe Blvd., Houston, TX 77030, USA

[5]Department of Veterinary Medicine and Surgery, The University of Texas M.D. Anderson Cancer Center, 1515 Holcombe Blvd., Houston, TX 77030, USA

[6]Department of Imaging Physics, The University of Texas M.D. Anderson Cancer Center, 1515 Holcombe Blvd., Houston, TX 77030, USA

[7]Department of Dermatology, The University of Texas M.D. Anderson Cancer Center, 1515 Holcombe Blvd., Houston, TX 77030, USA

[8]Department of Genetics, The University of Texas M.D. Anderson Cancer Center, 1515 Holcombe Blvd., Houston, TX 77030, USA

[9]Department of Molecular and Cellular Biology, Baylor College of Medicine, 1 Baylor Plaza, Houston, TX 77030, USA

[10]Department of Biology and Biochemistry, University of Houston, Houston, Texas 77204, USA

[11]Radiation Biology & Health Sciences Division, Bhabha Atomic Research Center, Mumbai-400085, India

[12]Correspondence to: Elsa R. Flores. (elsaflores@mdanderson.org).

AUTHOR CONTRIBUTIONS:

AV and ERF conceived the study, designed experiments, and analysed data. AV, PR, WN, DC, XS, SS, MSR, JL, CVK, EFS, KN JPT, JAB, and KYT designed and performed experiments. PHG, CC and KR performed bioinformatic analyses. ERF and AV wrote the paper. All authors discussed the paper and commented on the manuscript.

SUMMARY

TP53 is commonly altered in human cancer, and *Tp53* reactivation suppresses tumours *in-vivo* [1,2]. This strategy has proven difficult to implement therapeutically, and here we have examined an alternative strategy by manipulating the p53 family members, p63 and p73. The TA isoforms of *p63* and *p73* structurally and functionally resemble *p53*, while the ΔN isoforms of *p63* and *p73* are frequently overexpressed in cancer and act primarily in dominant negative fashion against p53, TAp63, and TAp73 to inhibit their tumour suppressive functions [3–8]. The p53 family interacts extensively in cellular processes that promote tumour suppression, such as apoptosis and autophagy[9–14], thus a clear understanding of this interplay in cancer is needed to treat tumours with alterations in the p53 pathway. Here, we show that deletion of the ΔN isoforms of p63 or p73 leads to metabolic reprogramming and regression of *p53* deficient tumours through upregulation of *IAPP*, the gene that encodes amylin, a 37 amino acid peptide cosecreted with insulin from the β cells of the pancreas. We found that *IAPP* is causally involved in this tumour regression and that amylin functions through the calcitonin receptor (CalcR) and receptor activity modifying protein 3 (RAMP3) to inhibit glycolysis and induce ROS and apoptosis. Pramlintide, a synthetic analog of amylin, which is currently used to treat type 1 and type 2 diabetes, caused rapid tumour regression in *p53* deficient thymic lymphomas, representing a novel strategy to target *p53*-deficient cancers.

Using Δ*Np63*[15] and Δ*Np73* conditional knock out mice (Extended Data Figure 1a & b), we generated Δ*Np63*+/− and Δ*Np73*−/− mice (Extended Data Figure 1c–f). To ask whether the ΔN isoforms of p63 and p73 act as oncogenes *in vivo* by interacting with p53, Δ*Np63*+/−;*p53*−/− and Δ*Np73*−/−;*p53*−/− mice were aged for the development of thymic lymphomas, which form in nearly all *p53*−/− mice[16]. We found a remarkable diminution in the number and size of thymic lymphomas in Δ*Np63*+/−;*p53*−/− and Δ*Np73*−/−;*p53*−/− mice leading to an extended lifespan (Extended Data Figure 2a–c) suggesting that the ΔN isoforms of p63 and p73 restrain a tumour suppressive program that can compensate for p53 function.

We found that TAp63 and TAp73 were upregulated in thymic lymphomas from Δ*Np63*+/−;*p53*−/− and Δ*Np73*−/−;*p53*−/− mice (Extended Data Figure 2d & e) along with an upregulation of apoptosis (Extended Data Figure 2f–j) and senescence (Extended Data 2k–o). We also examined thymocytes from 4 week old after treatment with 10 Gy gamma irradiation, a dose that is known to elicit p53-dependent apoptosis [9,17]. Indeed, TAp63 and TAp73 are higher in Δ*Np63*+/−;*p53*−/− and Δ*Np73*−/−;*p53*−/− thymocytes, which was further exacerbated after gamma irradiation (Extended Data Figure 3a–c) with an increase in apoptosis (Extended Data Figure 3d–h) and senescence (Extended Data Figure 3i–m).

To determine whether TAp63 or TAp73 compensate for p53 function in tumours *in-vivo*, we acutely remove Δ*Np63* or Δ*Np73* by intratumoral infection with adenovirus-cre-mCherry (Extended Data Figure 4a–d and Figure 1a–f) in Δ*Np63fl/fl;p53*−/− and Δ*Np73fl/fl;p53*−/− at 10 weeks of age. Tumours were 2.3–5.8 mm^3 in size at the time of infection and monitored weekly by MRI (Figure 1a–i). Mice deficient for either Δ*Np63* or Δ*Np73* and *p53* showed marked decreases in tumour burden (Figure 1h & i). The reduction of ΔNp63 and

ΔNp73 expression resulted in increased expression of TAp63 and TAp73 (Figure 1j–m and Extended Data 4d) and increased apoptosis (Extended Data Figure 4e–h) and senescence (Extended Data Figure 4i–k). Δ*Np63Δ/Δ;p53−/−* and Δ*Np73Δ/Δ;p53−/−* mice also had an increased lifespan (Figure 1n). We found differences in CD4/CD8 positive cells in young mice (4 weeks) (Extended Data Figure 4l–p) indicating that changes in T cell development may lead to a lower tumour incidence in double mutant mice. Indeed, we found that *p53−/−* thymic lymphomas are composed primarily of CD4/CD8 double positive thymocytes while the Δ*Np63Δ/Δ;p53−/−* and Δ*Np73Δ/Δ;p53−/−* lymphomas contain very few CD4/CD8 double positive thymocytes (Extended Data Figure 4q–t). Lastly, we asked whether thymic stromal cells contribute to the apoptosis in the regressing lymphomas. We sorted CD45 positive cells to select for T-lymphocytes in *p53−/−*, Δ*Np63fl/fl;p53−/−* and Δ*Np73fl/fl;p53−/−* mice and infected them with adenovirus-cre (Extended Data Figure 4u). Δ*Np63Δ/Δ;p53−/−* and Δ*Np73Δ/Δ;p53−/−* thymocytes underwent apoptosis independent of the presence of the stromal cells (Extended Data Figure 4v). These data indicate that inhibition of the ΔN isoforms of p63 and p73 serves to upregulate TAp63 and TAp73 to compensate for loss of p53 in tumor suppression.

We found that the ΔN isoforms of p63 and p73 bind to the promoters of the TA isoforms of *p63* and *p73* suggesting that the ΔN isoforms of p63 and p73 can transcriptionally repress TAp63 and TAp73 transcription (Extended Data Figure 5a–i). We also found that the increase in apoptosis and cellular senescence was dependent on TAp63 and TAp73 (Extended Data Figure 5j–q).

We performed RNA sequencing of lymphomas after infection with Ad-mCherry (Δ*Np63fl/fl;p53−/−* and Δ*Np73fl/fl;p53−/−*) and Ad-Cre-mCherry (Δ*Np63Δ/Δ;p53−/−* and Δ*Np73Δ/Δ;p53−/−*) and found that thymic lymphomas from mice deficient for *p53* and Δ*Np63* clustered with those from mice deficient for *p53* and Δ*Np73* (Extended Data Figure 6a). Ingenuity Pathway Analysis (IPA) (Figure 1q) revealed genes involved in metabolism including TP53-inducible glycolysis and apoptosis regulator (*TIGAR*)[18], and glutaminase 2 (*GLS2)*[19,20]. While we found that *TIGAR* and *GLS2* were upregulated in either Δ*Np63Δ/Δ;p53−/−* and Δ*Np73Δ/Δ;p53−/−* thymic lymphomas, we identified a novel gene, *islet amyloid polypeptide* (*IAPP*) or *amylin*, which limits glucose uptake resulting in increased intra-cellular glucose-6-phosphate (G-6-P) [21] and decreased glycolysis [21], to be upregulated by over 5 fold in both double mutant thymic lymphomas. We validated *IAPP*, *TIGAR*, and *GLS2* expression in thymic lymphomas derived from Δ*Np63Δ/Δ;p53−/−* and Δ*Np73Δ/Δ;p53−/−* mice and found that *IAPP* is expressed at levels over 2-fold higher in double mutant mice (Figure 1p and Extended Data Figure 6b–d). *IAPP* and *GLS2* depends on TAp63 and TAp73 (Figure 1q and Extended Figure 6d). To determine whether TAp63 or TAp73 transcriptionally regulate *IAPP*, we performed chromatin immunoprecipitation in MEFs (Extended Data Figure 6e–g) and thymocytes (Figure 1r & s). We found that TAp63 and TAp73 binds to sites located in the promoter (site 1), 1756 nucleotides upstream of the transcriptional start site, and intron 2 (site 2) of *IAPP*, 706 nucleotides downstream of the transcriptional start site (Extended Data Figure 6e–g). Because a greater binding affinity of TAp63 and TAp73 was detected in the promoter region (site 1) of *IAPP*, we cloned this site into a luciferase reporter gene and also mutated this site (Extended Data Figure 6h–k). Only

the luciferase reporter gene containing wild-type *IAPP* promoter site 1 was transactivated by TAp63 and TAp73 while the mutant version was not. Taken together, these data indicate that *IAPP* is a transcriptional target gene of TAp63 and TAp73 (Figure 1t).

Expression of IAPP in *p53−/−* MEFs resulted in low levels of glycolysis comparable to that in Δ*Np63−/−;p53−/−* and Δ*Np73−/−;p53−/−* MEFs (Extended Data Figure 6l–m & Figure 1u). Conversely, when we knocked down *IAPP* in Δ*Np63−/−;p53−/−* and Δ*Np73−/−;p53−/−* MEFs, the levels of glycolysis were similar to that of *p53−/−* MEFs (Figure 1u) indicating that IAPP inhibits glycolysis. *In vivo*, we detected massive tumour regression in Δ*Np63fl/fl;p53−/−* or Δ*Np73fl/fl;p53−/−* thymic lymphomas treated with IAPP (Extended Data Figure 7a and Figure 2a, b, h, i, o & p), $p<0.05$. Conversely, in Δ*Np63Δ/Δ;p53−/−* and Δ*Np73Δ/Δ;p53−/−* thymic lymphomas treated with Ad-shIAPP-mCherry the tumours continued to grow comparable to that of *p53−/−* thymic lymphomas (Figure 2a–k & o–r), $p>0.05$ at 13 weeks. Additionally, *p53−/−* mice treated with Ad-IAPP had an extended tumour free survival compared to *p53−/−* mice or Δ*Np63Δ/Δ;p53−/−* and Δ*Np73Δ/Δ;p53−/−* mice treated intratumourally with Ad-shIAPP-mCherry (Extended Data Figure 7a & b) indicating that *IAPP* is a tumour suppressor gene and is causally involved in the *in vivo* effects seen upon inactivation of ΔNp63 or ΔNp73. Given that pramlintide, a synthetic analog of amylin, is used to treat type I and type II diabetes [22], we treated thymic lymphomas in Δ*Np63fl/fl;p53−/−* or Δ*Np73fl/fl;p53−/−* mice. Indeed, 3 weekly intratumoral injections resulted in rapid tumour regression (Figure 2e, l, & s), $p<0.005$ at 13 weeks. This effect was exacerbated by systemic intravenous treatment with pramlintide (Figure 2f, m, & t and Extended Data Figure 7c–q), $p<0.005$ similar to that seen in tumors treated with a known inhibitor of glycolysis, 2DG, (Figure 2g, n, & u). These data provide preclinical *in vivo* evidence that pramlintide can be used to effectively treat *p53* deficient tumours. Using *in-vivo* dynamic magnetic resonance spectroscopy to measure the conversion of hyperpolarized [1-^{13}C]-pyruvate to lactate as a proxy of glycolysis within the tumours, we found a marked reduction in glycolysis in Δ*Np63/p53* and Δ*Np73/p53* double deficient mice and after introducing IAPP into *p53−/−* thymic lymphomas similar to tumors treated with 2DG (Figure 2v). Δ*Np63Δ/Δ;p53−/−* and Δ*Np73Δ/Δ;p53−/−* thymic lymphomas infected with an shRNA for IAPP exhibited levels of glycolysis similar to those found in *p53−/−* thymic lymphomas (Figure 2v). Pramlinitide also inhibits glycolysis in tumours (Figure 2v).

IAPP has been shown to induce ROS and activate apoptosis [23,24]. We found a drastic increase in the levels of ROS and apoptosis in thymic lymphomas expressing IAPP, pramlintide, or 2DG while both ROS and apoptosis did not occur upon inactivation of *IAPP* in thymic lymphomas from Δ*Np63Δ/Δ;p53−/−* and Δ*Np73Δ/Δ;p53−/−* mice (Figure 2w) indicating that upregulation of IAPP inhibits glycolysis similar to 2DG and leads to oxidative stress that triggers apoptosis. While high levels of ROS are not commonly triggered by inhibition of glycolysis, nutrient deprivation or excess can result in the accumulation of ROS. Additionally, cancer cells tightly regulate ROS by acquiring additional mutations and compensatory mechanisms often ensue and may be at play in the thymic lymphoma cells that acutely downregulate glycolysis by IAPP[25].

To extend our findings to human cancer where p53 is altered in the majority of cases, we analyzed human cancer cell lines containing p53 deletions or mutations. We used siRNA to knockdown ΔNp63 or ΔNp73 in cells derived from a lung adenocarcinoma (H1299) (Figure 3a). Down regulation of Δ*Np63* or Δ*Np73* resulted in upregulation of TAp63, TAp73, and IAPP (Figure 3a) and an increase in apoptosis and decrease in cell proliferation (Figure 3b and Extended Figure 8a–d). To ask whether IAPP can also inhibit glycolysis in human cancer cell lines, we transfected H1299 cells with siΔNp63, siΔNp73 or IAPP (Figure 3a). Knock down of ΔNp63 or ΔNp73 or expression of IAPP resulted in an inhibition of glycolysis (Figure 3c & d) and glucose uptake (Extended Data Figure 8e & g), accumulation of ROS (Figure 3d–f), and induction of apoptosis (Figure 3d, g & h). We inhibited ROS in these cells using N-acetyl-L-cysteine (NAC) and observed no apoptosis (Figure 3d–h). Previous studies have indicated that IAPP inhibits glycolysis by increasing intracellular glucose-6-phosphate (G-6-P) in turn leading to an inhibition of hexokinase [21,26]. We measured the levels of intracellular G-6-P in H1299 cells and found that cells expressing high levels of IAPP (H1299-siΔNp63, H1299-siΔNp73, or H1299+IAPP) also had high levels of G-6-P while knock down of IAPP resulted in a diminution in G-6-P (Extended Data Figure 8f & g). Over expression of glucose hexokinase II (HKII) led to a rescue of the glycolytic capacity of H1299 cells expressing siΔNp63 or siΔNp73 similar to levels in parental H1299 cells (Figure 3c–g). These results indicate that IAPP inhibits glycolysis through the inhibition of HKII. We found that treatment of H1299 cells with pramlintide led to similar effects on glycolysis and apoptosis (Figure 3g–n). Taken together, these data demonstrate that IAPP and pramlintide inhibit glycolysis through the inhibition of HKII.

IAPP is a secreted protein and binds to the calcitonin receptor (CALCR) and receptor activity modifying protein 3 (RAMP3)[27]. To determine whether IAPP functions through these receptors to inhibit glycolysis, secreted media from H1299 cells expressing siΔNp63 (siΔNp63^{M}) or siΔNp73 (siΔNp73^{M}), which contains secreted IAPP (Figure 4a and Extended Figure 9a & b), was added to H1299 cells resulting in inhibition of glycolysis (Figure 4b) and induction of ROS and apoptosis (Figure 4c & d). In contrast, when these media were used to treat H1299 cells with knock down of CALCR or RAMP3, glycolysis was not inhibited and ROS and apoptosis were not induced (Figure 4b–d) indicating that the CALCR and RAMP3 receptors are critical for IAPP function. We also treated the H1299 cells with media from H1299 cells expressing siΔNp63 (siΔNp63^{M}) or siΔNp73 (siΔNp73^{M}) and an amylin inhibitor (A.I.), which led to high levels of glycolysis (Extended Data Figure 9c) and low levels of ROS and apoptosis (Figure 4c & d). IAPP causes activation of the NLRP3 inflammasome [28], which has been shown to be anti-tumourigenic in certain cancers via IL-18 processing[29]. We blocked caspase-1 using an inhibitor and found that it prevented apoptosis of H1299 cells (Figure 4d), demonstrating that pyroptosis may also be an important mechanism of action of IAPP.

To demonstrate the importance of the calcitonin receptor *in vivo*, we treated *p53−/−* mice with thymic lymphomas at 10 weeks of age with pramlintide and a calcitonin receptor inhibitor (Figure 4e–m) and found this inhibition rendered pramlintide ineffective indicating the importance of the calcitonin receptor for IAPP/amylin/pramlintide function (Figure 4n). To further determine the anti-tumourigenic efficacy of pramlintide in cells with p53

deletions or mutations, we treated additional human cancer cell lines [30] with pramlintide and a calcitonin receptor inhibitor resulting in increased glycolysis, decreased ROS and apoptosis (Extended Data Figure 9d–i). We assessed patient survival using data from the Cancer Genome Atlas (TCGA) of patients with p53 mutations and found that co-expression of IAPP, CALCR and RAMP3 correlated with better patient survival in basal breast cancer (Figure 4o), and colorectal cancer and lung squamous cell carcinoma (Extended Data Figure 9j & k).

Reactivation of p53 activity in tumours results in tumour suppression[1,2]. We have focused on interactions between the three p53 family members and have revealed a novel strategy to target *p53*-deficient and mutant cancers through amylin based therapies like pramlintide.

METHODS

Generation of ΔNp73 Conditional Knockout Mice

The cre-loxP strategy was used to generate the Δ*Np73* conditional knockout allele (Δ*Np73fl*). Genomic *p73* DNA from intron 3 to intron 3′ was amplified from BAC clone DNA (BAC RP23-186N8, Children's Hospital Oakland Research Institute). LoxP sites flanking exon 3′ of *p73* and neomycin (*neo*) gene flanked by frt sites inserted in intron 3′ were cloned into pL253 [31]. Mouse embryonic stem cells (G4) electroporated with the targeting vector were analyzed by Southern blot analysis for proper targeting of the Δ*Np73* allele. Resulting chimeras were mated with C57BL/6 albino females and genotyped as described below. Mice with germ line transmission of the targeted allele (conditional, flox neo allele, fn) were crossed to the FLPeR mice to delete the neo cassette. Resulting progeny were intercrossed with Zp3-Cre (C57BL/6)[32] transgenic mice. Δ*Np73fl/+; Zp3-Cre* females were mated with C57BL/6 males to generate Δ*Np73*+/− mice. The Δ*Np73*+/− mice were intercrossed to generate Δ*Np73*−/− mice. Compound mutant mice were generated by intercrossing the Δ*Np63*+/− and Δ*Np63fl/fl*[15] and the Δ*Np73*−/− and Δ*Np73fl/fl* mice with the *p53*−/− mice [16]. All procedures were approved by the IACUC at U.T. M.D. Anderson Cancer Center.

Genotyping

Genomic DNA from tail biopsies was genotyped by Southern blot analysis by digesting genomic DNA with AflII and HindIII or by PCR using the following primers and annealing temperatures: 1) for wild-type: wt-F, 5′-ACAGTCCTCTGCTTTCAGC-3′ and wt-R (fl-R), 5′-CACACAGCA CTGGCCTTGC -3′, annealing temp: 58°C, 2) for ΔNp73flox: fl-F, 5′ –CATAGCCATGGGCTCTCCT - 3′ and fl-R (wt-R), 5′–TGTCCTGCTGCTGGTTGTAT-3′, annealing temp: 63°C, 3) ΔNp73floxneo: flneo-F, 5′-GGGAGGATTGGGAAGACAAT-3′ and flneo-R, 5′-TGTCCTGCTGCTGGTTGTAT-3′ annealing temp:60°C and 4) for ΔNp73KO: ko-F, 5′-CCTAGCCCAAGCATACTGGT-3′ and wt-R, 5′-TGTCCTGCTGCTGGTTGTAT-3′ annealing temp: 58°C. Primers used to genotype for the Cre gene are as follows: Cre-F, 5′–TGGGCGGCATGGTGCAAGTT-3′ and Cre-R, 5′–CGGTGCTAACCAGCGTTTTC-3′, annealing temp: 60° C. The primers for ΔNp63WT, ΔNp63KO, ΔNp63flox and p53 were previously described[15,16].

Cell Lines

Mouse embryonic fibroblasts (MEFs) for the indicated genotypes were generated as described previously[9]. Human lung adenocarcinoma cells (H1299), colorectal adenocarcinoma cells (SW-480) and breast adenocarcinoma cells (MDA-MB-468) were purchased from ATCC and cutaneous SCC cell lines (SRB12, COLO16)[30] were a gift from Dr. K. Y. Tsai. The MEF's, SW-480 and MDA-MB-468 cells were cultured in DMEM (Cellgro) and H1299 cell lines were cultured in RPMI 1640 (Cellgro). The SRB12 and COLO16 cell lines were grown in DMEM/Ham's F12 50/50 (Cellgro). All cell lines used in the study tested negative for mycoplasma.

Immunhistochemistry

Mice thymic lymphomas or thymii were dissected, fixed in 10% formalin, and embedded in paraffin. Sections were dewaxed in xylene and re-hydrated using decreasing concentrations of ethanol. Antigens were unmasked in citrate buffer unmasking solution (Vector Laboratory) followed by incubation with blocking solution, and 18 hour incubation at 4°C with the following antibodies: cleaved caspase 3 (1:200)(Cell Signaling), PCNA (1:500) (Cell Signaling), malondialdehyde (1:50)(Abcam). Visualization was performed using the ImmPact DAB peroxidase substrate kit (SK4105, Vector Laboratories) and counter-stained with Hematoxylin (H-3401, Vector Laboratories). The slides were mounted using VectaMount (H-5000, Vector Laboratories). Images were acquired using a Zeiss Axio microscope and analyzed with ProgRes Capture Pro 4.5 software.

SA-β-gal staining

SA-β-gal staining on mouse thymic lymphoma was performed as described previously [33].

Quantitative real time PCR

Total RNA was prepared from MEFs or mouse tissues using TRIzol reagent (Invitrogen)[4,8,34]. cDNA was synthesized from 5μg of total RNA using the SuperScript® III First-Strand Synthesis Kit (Invitrogen) according to the manufacturer's protocol followed by qRT PCR using the SYBR Fast qPCR master mix (Kapa Biosystems). qRT-PCR was performed using a ABI 7500 Fast Real-time PCR machine. Primers for mouse *TAp63*, Δ*Np63*, *PUMA*, *Noxa*, *bax*, *PML*, *p16* and *p21*[4,34] and human *TAp63*, Δ*Np63* and *GAPDH* were used as described previously [4,34]. Human primers for *PUMA*, *Noxa*, *bax*, *PML*, *p16*, *p21* were used as described previously [33] and *GLS2* and *TIGAR* as described previously [19]. Mouse primers for *TAp73* are FOR:5′-GCACCTACTTTGACCTCCCC-3′, REV: 5′-GCACTGCTGAGCAAATTGAAC-3′, Δ*Np73* are FOR: 5′-ATGCTTTACGTCGGTGACCC-3′, REV: 5′-GCACTGCTGAGCAAATTGGAAC-3′, *IAPP* are FOR: 5′-CTCCAAACTGCCATCTGAGGG-3′, REV: 5′-CGTTTGTCCATCTGAGGGTT-3′. Human primers used for *TAp73* are FOR: 5′-CAGACAGCACCTACTTCGACCTT-3′, REV: 5′-CCGCCCACCACCTCATTA-3′ and for Δ*Np73* are FOR: 5′-TTCAGCCAGTTGACAGAACTAAG-3′, REV: 5′-GGCCGTTTGTTGGCATTT-3′.

Western blot analysis

Fifty micrograms of protein were electrophoresed on a 10% or 15% SDS PAGE and transferred to PVDF membrane as described previously [4,8,34]. Blots were probed with anti-p63 (1:500) (4A4, Santa Cruz), anti-TAp63 (1:1000) (BioLegend), anti-TAp73 (1:500) (IMG-246, Imgenex), anti-p73 (Mouse) (1:250)(IMG-259A, Imgenex), anti-p73 (1:1000) (human) (EP436Y, Abcam), anti-p53 (WT) (1:1000)(CM5, Vector Labs), anti-IAPP (1:1000)(ab103580, Abcam), anti-His (1:1000)(G18, Santa Cruz), anti-Hexokinase II (1:10000)(C64G5, Cell Signaling), anti-calcitonin receptor (1:1000)(ab11042, Abcam), RAMP3(1:1000)(H125, Santa Cruz), and cleaved caspase 3 (1:1000)(Asp 175, Cell Signaling), at 4°C for 18 hours followed by incubation for one hour at room temperature with the appropriate secondary antibodies conjugated to horseradish peroxidase (1:5000) (Jackson Lab). β-actin (Sigma 1:5000) was used as a loading control. Detection was performed using the ECL Plus Kit (Amersham) following the manufacturer's protocol and x-ray autoradiography.

Characterization of thymus using flow cytometry

Thymii from 4 week old mice and thymic lymphomas from 10 week old mice were collected 48 hours after adenovirus infection. Single cells were obtained by homogenizing the thymii through a 0.75 μM filter. Cells were stained with CD3-PE (145-2C11), CD4-PerCP-Cy5.5 (RM4-5), CD8-APC (53-6.7), CD45-FITC (30-F11)(BDPharmingen), AnnexinV-Pacific Blue (A35122, Life Technologies), and 7-AAD (V35124, Invitrogen) and sorted using a BD Aria Cell Sorter or analyzed using the LSR Fortessa Cell Analyzer and FlowJo software.

Chromatin Immunoprecipitation (ChIP)

MEFs were grown to near confluence at passage 2 on DMEM media with 10% serum as previously described [9]. Thymocytes from 6-week-old mice were collected 48 hours after adenovirus infection. Cellular proteins were cross-linked to DNA using 1% formaldehyde and chromatin was prepared as described previously [4,8,34]. TAp63 and ΔNp63 ChIP analysis was performed using a pan-p63 antibody (4A4, Santa Cruz) as described previously and the TAp73 ChIP was performed using a TAp73 antibody (ab14430, Abcam) and ΔNp73 ChIP was performed using a p73 antibody (IMG 259A, Imgenex). Putative TAp63 and TAp73 binding sites were scanned 3000bp upstream of the 5′UTR and in intron 2 of the IAPP gene. qRT–PCR was performed by using primers specific for the indicated regions of *IAPP*: Promoter-Site 1 (−1802) -forward 5′-AGAGTTCAAGGTCATCCTCGAC-3′ and (−1731) - reverse 5′-TGTTCTGACATGCAGCCTCA-3′, Intron-2- Site 2 (+678)-forward 5′-AGACAGGCATGCTTAGAGACG-3′ and (+765)– reverse 5′-CACTCAGTGTGGATGTCCGT-3′, and non-specific site (+7532)- forward 5′-GTGTGTGATGGTTTGGTGGAT-3′ and (+7623) - reverse 5′-ACAAGGCAGTTGATGGAGACT-3′. Similarly, putative ΔNp63 and ΔNp73 binding sites were scanned 10000 bp upstream of the 5′UTR and in intron 1 of *TAp63* and *TAp73*. qRT-PCR was performed by using the primers specific for the indicated regions on the *TAp63* promoter: Site 1 (−41) –forward 5′-CAGGAGCTCTCAAATCAAGTCAGA-3′ and (+37) – reverse 5′-ATCACAGAAGCCAGGACTTGTCAC-3′, and non-specific site (−3030) - forward 5′-GCTATAAATGTTTCCATGTGATGGATTGC-3′ and (−2973) - reverse 5′-

TGCAGACTTAGCTATGGTCTCTTG-3′. Similarly, qRT-PCR was performed using the primers specific for the indicated regions on the *TAp73* promoter: Site 1 (−1103) –forward 5′-CTAGCACACCAATCCAAGGAAAGA and (−1059) –reverse 5′-GCCTGCAGTCCGGGTTT-3′ and non-specific site (−2488)–forward 5′ACTAGACCTCTGTACTTGTGAACATACATTT-3′ and (−2382) –reverse 5′-GCACTCTCAFFATCCTGTAACAAAA-3′.

Dual luciferase reporter assay

Luciferase assays were performed using *p53−/−;p63−/−* and *p53−/−;p73−/−* MEFs as described previously[35]. To generate the luciferase reporter gene (pGL3-IAPP), the DNA fragment containing the TAp63/TAp73-binding site identified by ChIP was amplified from C57BL/6 genomic DNA by PCR with the following primers containing 5′ XhoI and 3′ HindIII cloning restriction enzyme sites: IAPP 5′-ATACTCGAGGTGTTCAGGGAACCTTCGGT-3′ (forward) and 5′-ATAAAGCTTCACCTGACCTCCAAACTCCC-3′ (reverse). Similarly, a mutant version of the luciferase reporter gene (pGL3-IAPP^{Mut}) was generated using QuikChange Lightning (Agilent Technologies) following the manufacturer's instructions. The following primers 5′-TATTGTTCTGACATCCAGCCTGATGTTGCCCAGTCTGGT-3′ (forward) and 5′-ACCAGACTGGGCAACATCAGGCTGGATGTCAGAACAATA-3′(reverse) were used to generate the mutant version.

Reverse Transfection

Cells were transfected with 50 nM siΔNp63 (SASI_Hs02 00328367)(Mission siRNA, Sigma), siΔNp73 (SASI_Hs02_00326884)(Mission siRNA, Sigma), siTAp63 (SASI_Hs01_00246771) (Mission siRNA, Sigma), siTAp73 (SASI_Hs02_00339573) (Mission siRNA, Sigma), siRAMP3 (SASI_Hs01_00199036)(Mission siRNA, Sigma), siCalcitonin receptor (SASI_Hs01_00077738)(Mission siRNA, Sigma), siIAPP (SASI_Hs01_00183962) (Mission siRNA, Sigma) or siNT(SIC_001)(Mission siRNA, Sigma) using Lipofectamine RNAiMAX (Invitrogen). The mixture of siRNA and Lipofectamine were combined together and added to the well followed by the addition of 200,000 cells/well in a 6-well dish.

Transfections - Generation of IAPP and Hexokinase II expressing cells

3×10^5 cells were plated in 10cm dishes. MEFs and human cancer cells were transfected with 8 μg Myc-DDK-IAPP (RC215074)(Origene) or 3.3μg HKII (Plasmid #25529)(Addgene) using X-tremeGENE HP (Roche) and incubated for 48–60hrs. Cells were selected with G418, MEFs (350μg/μl) and human cancer cells (500μg/μl) for a period of 9 days.

Secreted IAPP Protein concentration

Twelve hours after knockdown of ΔNp63/ΔNp73 in human cancer cells, fresh serum free media was added to the cells. Following a sixty-hour incubation, the media was collected and concentrated using Amicon Ultra-15 Centrifugal Filter Units (UFC901008, EMD Millipore).

RNA Sequencing and Analysis

Five μg of polyA+ RNA were used to construct RNA-Seq libraries using the standard Illumina protocol. Mouse mRNA sequencing yielded 30–40 million read pairs for each sample. The mouse mRNA-Seq reads were mapped using TopHat [36] onto the mouse genome and build UCSC mm9 (NCBI 37) and the RefSeq mouse genes. Gene expression and gene expression differences were computed using Cufflinks[36]. For each species, a combined profile of all samples was computed; mRNA abundance was mean-centered and Z-score transformed for each mRNA individually. Principal component analysis was executed using the implementation within the R statistical analysis system. Hierarchical clustering of samples was executed by first computing the symmetrical sample distance matrix using the Pearson correlation between mRNA profiles as a metric, supervised sample analysis was performed using the t-test statistics, and heatmaps were generated using the heatmap.2 package in R. For gene signatures and pathway analysis gene list from the RNA-Seq comparing Δ*Nfl/fl;p53*−/− versus Δ*Np63Δ/Δ;p53*−/− and Δ*Np73Δ/Δ;p53*−/− were obtained at a p-value <0.01. The RNA-Seq data has been deposited in the Gene Expression Omnibus (GEO) data repository and can be accessed using the following database accession number: GSE60827. The genes upregulated in the Δ*Np63Δ/Δ;p53*−/− and Δ*Np73Δ/Δ;p53*−/− and down regulated in the Δ*Nfl/fl;p53*−/− were selected. The relative fold change of the genes were calculated and sorted from highest to lowest. Genes with a greater than 1.5 fold-increase were selected and run through the Ingenuity Pathway Analysis (IPA) (Ingenuity Systems) to screen for pathways and processes. Genes from the selected pathways were cross-referenced with the Gene Set Enrichment (GSEA)(Broad Institute) data analysis, DAVID Bioinformatics Resource 6.7 and GSEA implementation at the Molecular Signature Database (MSigD) [37].

Magnetic Resonance Imaging

MRI imaging was performed at 10 weeks of age when the tumours were established and the volumes range from 2.3 mm^3 to 5 mm^3. To reduce the variation between different groups of mice, a cohort of n=5 with similar tumour volumes was established and tumors regression was monitored by MRI. All mice were scanned once a week for a period of 35 weeks on a 7-Tesla, 30-cm bore BioSpec MRI system (Bruker Biospin Corp., Billerica, MA).

Hyperpolarized Magnetic Resonance Spectroscopy

Dynamic MR spectroscopy (MRS) of hyperpolarized (HP) [1-^{13}C] pyruvate was performed *in vivo* in tumour bearing mice. To achieve polarization, a 26-mg sample of pyruvic acid (Sigma-Aldrich, St. Louis, MO) with 15 mM of OX063 radical (GE Healthcare, Waukesha, WI) and 1.5-mM Prohance (Bracco Diagnostics Inc., Monroe Township, NJ) was polarized in a HyperSense DNP system (Oxford Instruments, Abington, Oxfordshire, UK) as previously described [38,39]. The frozen sample was dissolved in a 4-mL buffer containing 40-mM TRIS, 80-mM NaOH, and 50-mM NaCl, resulting in a final isotonic and neutral solution containing 80-mM [1-^{13}C] pyruvate. A dual-tuned 1H/13C linear RF volume coil with 72mm ID was used in conjunction with imaging gradients with 12cm ID. For anatomic imaging, the ^{1}H channel was used in transmit/receive mode. In addition to localizing scans, flow-weighted oblique gradient echo images (TE = 1.4ms; TR = 55ms; 90° excitation; 3cm

× 3cm FOV encoded over a 64 × 64 image matrix) were acquired to confirm that the slice prescription for 13C measurements would not be obfuscated by signals originating from within the heart. For carbon spectroscopy, the RF volume coil was used in transmit-only mode in conjunction with a custom-built 15-mm ID ^{13}C surface coil for signal reception. After dissolution, 200 μL of the HP [1-^{13}C] pyruvate solution was administered to the animals via tail-vein catheter. A slice-selective pulse-acquire sequence (TR = 1,500 ms; 15° flip angle; 5 KHz spectral bandwidth; 2048 spectral points; 8-mm oblique slab; 120 repetitions) was used for dynamic spectroscopy beginning approximately 15s prior to injection. Data were processed to generate spectral time-courses of the HP-pyruvate and its lactate product. Spectra were phase adjusted and the area under the spectral peaks associated with [1-^{13}C] pyruvate and [1-^{13}C] lactate were integrated over time to reflect the overall signal observed from each metabolite over the course of the measurement. Total lactate signal, which could only arise from interaction of HP pyruvate with relevant metabolic enzymes, was normalized to the total signal from pyruvate.

Glycolysis Stress Assay

Extra-cellular acidification rate (ECAR) was measured using the extracellular flux analyzer (SeaHorse Bioscience XF96) following the manufacturer's instructions. Forty-eight hours after transfection, the cells were plated at a density of 1.5×10^4 cells per well in the XF 96-well cell culture plates. Twenty-four hours after seeding, the culture medium was replaced with 180 μl of running medium and incubated for 1 hour at 37°C in a non-CO_2 incubator. Before calibration, 20 μl of 50 mM glucose, 11 μM oligomycin and 650 mM 2-DG were aliquoted into each port in the sensor cartridge. ECAR was measured after the addition of glucose and oligomycin and before the addition of 2-DG. Extra-cellular acidification rate was normalized to mpH/min.

Glucose Uptake Measurement

Glucose uptake was calculated as a measure of glucose dependent proton secretion from the maximum and basal glucose consumption after addition of 20 μl of 50 mM glucose and measured using the extracellular flux analyzer (SeaHorse Biosciences XF96).

Glucose-6-phosphate Assay

Glucose-6-phosphate was measured using the Glucose-6-phosphate assay kit (ab83426, Abcam) following the manufacturer's instructions. Forty-eight hours after transfection, 2×10^6 cells were collected, homogenized and passed through a 10 kD spin-column filter. The eluate was collected and glucose-6-phosphate enzyme and substrate reaction was performed for 30 min and absorbance was measured at 450nm.

Proliferation Assay

The transfected human cancer cells were plated at a density of 5×10^3 cells in 6 replicates in a 96-well dish. Twelve hours later, the cells were labeled with 10 mM EdU (5′-ethynyl-2′-deoxyuridine) for a period of 8 hours. The assay was performed using the Click-iT EdU microplate assay (Invitrogen). Images were obtained using a Zeiss Axio fluorescent microscope and analyzed using the AxioVision Image 4.5 software.

Apoptosis Assay

Cells were plated at a density of 1×10^4 cells in 6 replicates in a 96-well dish. Twelve hours later, the cells were washed with 1X Annexin binding buffer and a cocktail of 5μl Annexin V-Alexa Fluor 488 for 100μg/ml propidium iodide (PI) and 2μg/ml Hoechst 33342 (Invitrogen) was added. Images were captured using the Zeiss fluorescent microscope and Axiovision Image 4.5 software. Quantification of the percent apoptosis was obtained using a high-throughput immunofluorescence plate reader (Celigo).

ROS Assay

Cells were plated at a density of 1×10^4 cells in 6 replicates in 96-well dish. Twelve hours later, the cells were incubated with a cocktail of 5 μM concentration of CellROX Deep Red Reagent (C10422, Invitrogen) and 2 μg/ml Hoechst 33342(Invitrogen) for 45 minutes at 37°C. Images were captured using a Zeiss fluorescent microscope and Axiovision Image 4.5 software. Quantification of the percent ROS was obtained using a high-throughput immunofluorescence plate reader (Celigo)[40].

In vitro Adeno-Cre Infection

Δ*Np63fl/fl;p53−/−* and Δ*Np73fl/flp53−/−* MEFs were plated at a density of 2.5×10^5 cells in 10 cm dishes before infection. Twelve hours later, MEFs were infected with Adeno-CMV-mCherry or Adeno-CMV-Cre-mCherry (Gene Transfer Vector Core Facility, University of Iowa). The cells were infected at an MOI of 6000 particles/cell. The efficiency of infection was quantified by assessing mCherry positive cells.

In vivo Adeno-virus Infection and IVIS Lumina Imaging

All mice were anesthetized using isoflurane and 2% oxygen and placed on a custom bed. An incision was performed to expose the sternum. Using a 28.5G U100 Insulin syringe, Adeno-mCherry/Adeno-Cre-mCherry (Gene Transfer Vector Core Facility, University of Iowa), Adeno-IAPP-mCherry(Vector Labs) or Adeno-shIAPP-U6-mCherry (TRCN0000416196, Mission shRNA)(Vector Labs) (sequence - CCGGTGTAAATTCTCATGCTAAGAACTCGAGTTCTTAGCATGAGAATTTACATTTTTTG) was surgically administered by intra-thymic injection (5×10^{12} viral particles/gram of body weight) through the 2nd and 3rd sternum. The incision was sealed using wound clips and mice were allowed to recover. To determine the efficiency of the *in vivo* viral delivery to the thymic lymphoma, IVIS Lumina Imaging (Perkin Elmer) was performed 48 hours later. Images were captured using a Mid-600 series bandwidth filter and analyzed using the Living Image® data analysis software.

shRNA Knockdown

shRNA plasmids for Trp63 (Clone ID: V3LMM_508694) (sequence - TGATCTTCAGCAACATCTC) and Trp73 (Clone ID: V3LMM_438557) (sequence - TGCAGGTGGAAGACATCCA) were obtained from the MD Anderson shRNA core facility (Open Biosystems). 293T cells were plated at a density of 2.5×10^5 cells in 10 cm dishes. Three micrograms of shRNA and packaging vectors were transfected as described previously [4]. Cells were selected using puromycin (3 μg/ml) for 7 days.

In vitro and in vivo administration of 2-Deoxy-D-glucose

1×10^4 cells were plated in 6 replicate wells in a 96-well dish. Twelve hours later, the human cancer cells were treated with 50 mM final concentration of 2-Deoxy-D-glucose (2-DG) (D8375-5G, Sigma) for 1 hour. Similarly, 2-DG (500 mg/kg of tumour weight)(D8375-5G-Sigma) was administered directly into the lymphoma of mice as described earlier[39].

N-acetyl-L-cysteine treatment

1×10^4 cells were plated in 6 replicate wells in a 96-well dish. Twelve hours later, cells were treated with N-acetyl-L-cysteine (NAC) (2 mM)(A8199, Sigma) final concentration for a period of 1 hour.

Amylin and caspase inhibitor treatment

2×10^5 cells were plated in triplicate in a 6-well dish. Twelve hours later, cells were treated with Amylin peptide (5μM) (A5972, Sigma) or with a Caspase 1 inhibitor (20μM)(Z-YVAD-FMK-218746, Calbiochem) for a period of 48 hours.

In vitro and in vivo administration of pramlintide acetate

2×10^5 cells were plated in duplicate in a 6-well dish. Twelve hours later, cells were treated with 10 μg/ml pramlintide acetate (AMYLIN Pharmaceuticals) or placebo for a period of 48 hours. pramlintide acetate (AMYLIN Pharmaceuticals) or placebo (sodium acetate/acetic acid) was surgically administered through non-invasive intra-thymic injection using a multiple dose protocol of pramlintide acetate (30 μg/gram of tumour weight). One injection per week for three weeks was administered directly into the thymic lymphoma of the animal. Another cohort of mice was treated bi-weekly for 3 weeks by intra-venous (I.V.) tail-vein injection of pramlintide acetate (45 μg/kg body weight) or placebo. The investigator was blinded to the treatment administered to each mouse. Tumour volumes were monitored weekly by MRI. Health and blood glucose levels of the treated animals were monitored weekly.

In vitro and In vivo administration of calcitonin receptor antagonist

2×10^5 cells were plated in duplicate in a 6-well dish. Twelve hours later, cells were treated with Calcitonin receptor antagonist (1 nM)(AC187, Tocris Bioscience) for a period of 48 hours with or without simultaneous pramlintide treatment. Similarly, a chronic dose of Calcitonin receptor antagonist (1 nM/gram of tumour weight) was administered through non-invasive intra-thymic injections with one injection every week for a period of three weeks with or without simultaneous pramlintide treatment. Tumour volume was monitored and measured weekly by MRI.

Survival Analysis

Survival analysis was conducted for the IAPP, RAMP3 and CalCR gene in the following datasets: the Memorial Sloan Kettering Cancer Center and the TCGA Cancer cohort. We considered four major cancer types with high p53 mutation rates, which include lung squamous cell carcinoma[41], head & neck squamous cell cancer[42,43], basal breast cancer[44,45], and colon cancer[46]. The co-expression of the three genes was analyzed in cases only with

p53-mutation. In all cases, we considered gene expression changes above or below 2 standard deviations with respect to the normal controls. The log-rank test and Cox P test was used to assess significance between the samples with or without expression changes of the IAPP, RAMP3 and CalCR gene using the cBioPortal for cancer genomics[47].

Statistics

Sample size for mouse cohorts in each experiment was chosen based on the penetrance of the thymic lymphoma phenotype of the *p53−/−* mouse model (80%). Twenty to thirty mice were used for survival analyses. Data were analysed using a one-way ANOVA test or a Student's t-test (two-sided) was used for comparison between two groups of data. A p-value of 0.05 was considered significant. Data are represented as mean ± s.e.m.

Extended Data

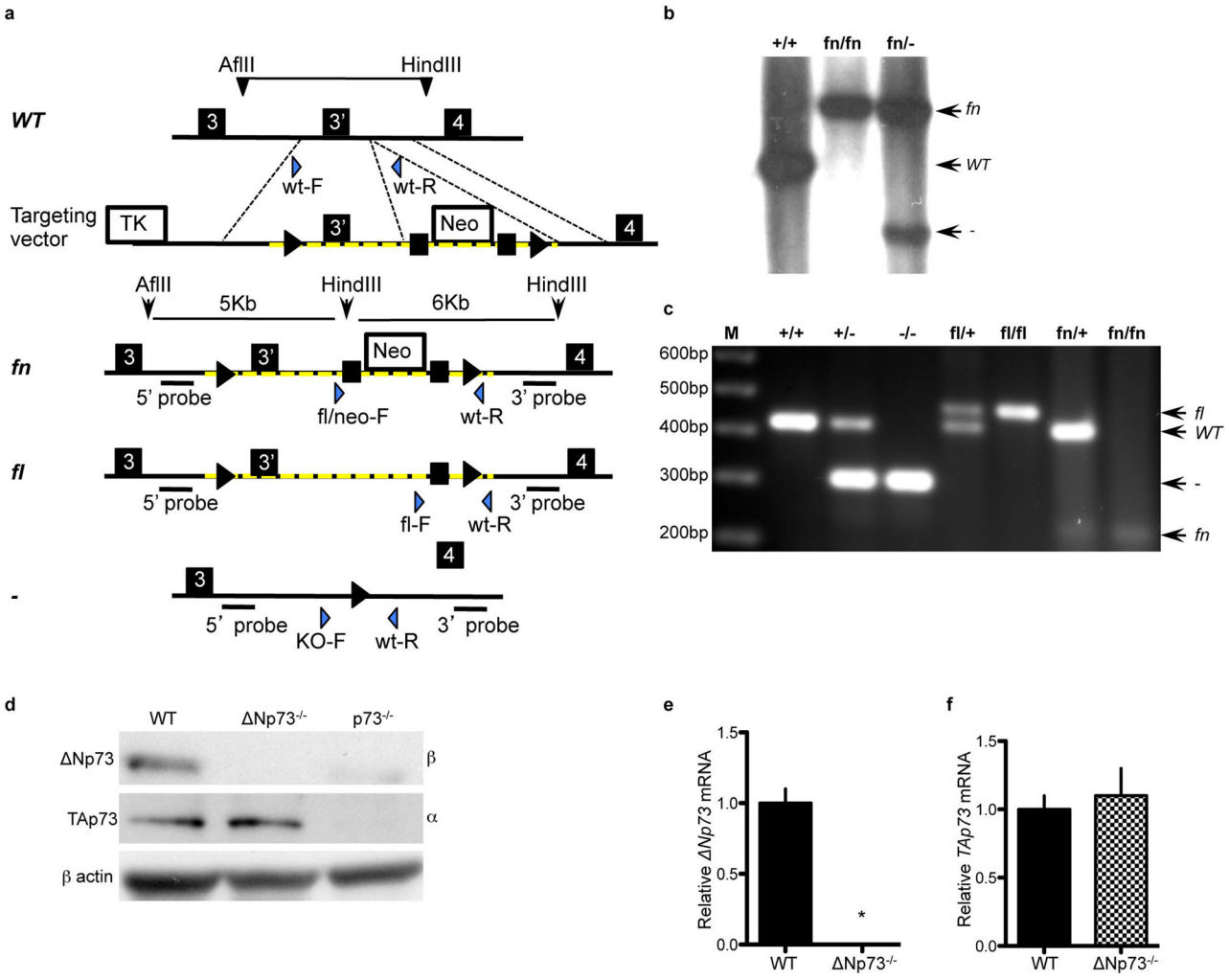

Extended Data Figure 1. Generation and characterization of Δ*Np73* conditional knock out mice

The ΔNp73 targeting vector was generated by inserting loxP sites (triangles) flanking exon 3′ and a neomycin cassette (neo) flanked by frt sites (squares) (**a**). The location of PCR

primers in each allele is shown by blue arrows. The targeted region of the floxed allele is depicted by yellow-dashed lines. Southern blot analysis using the 5′ probe shown in (**a**) and tail genomic DNA derived from mice of the indicated genotypes (**b**). PCR analysis using tail genomic DNA of the indicated genotypes (**c**). Western blot analysis using mouse embryo fibroblasts (MEFs) of the indicated genotypes (**d**). Q-RT-PCR in MEFs of the indicated genotypes (**f**), n=4, p<0.005. Statistical significance is indicated by black asterisks.

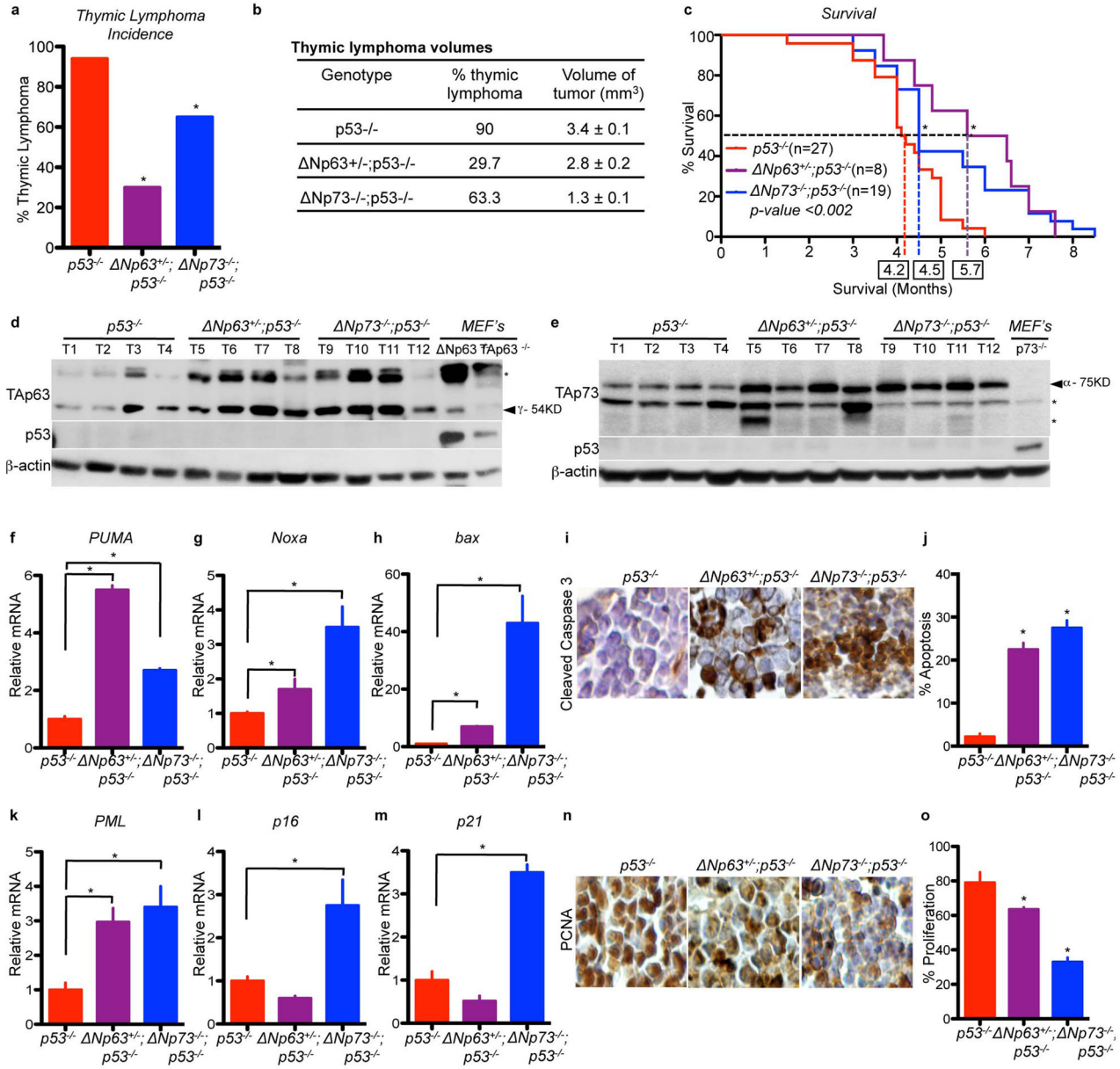

Extended Data Figure 2. Decreased thymic lymphomagenesis and increased survival in mice double deficient for Δ*Np63* and *p53* or Δ*Np73* and *p53*.

Quantification of thymic lymphoma incidence (n=30 mice) (**a**). Table showing thymic lymphoma volumes. The difference in tumour volumes between *p53−/−* and Δ*Np63+/−;p53−/−* and *p53−/−* and Δ*Np73−/−;p53−/−* was statistically significant with p values of

<0.03 and <0.002 respectively (**b).** Kaplan Meier survival in mice (**c**). Boxed numbers indicate median survival. Western blot analysis of thymic lymphomas of the indicated genotypes. Arrows indicate specific isoforms. Asterisks indicate non-specific bands (**d & e**). Q-RT PCR for *PUMA* (**f**), *Noxa* (**g**), and *bax* (**h**) in thymic lymphomas of the indicated genotypes, n=4, p<0.005. Immunohistochemistry (IHC) for cleaved caspase 3 in thymic lymphomas (**i**). Quantification of apoptosis as assessed by cleaved caspase 3 staining (**j**), n=20 fields of 3 biological replicates, p<0.005. Q-RT PCR for *PML* (**k**), *p16* (**l**), and *p21* (**m**) in indicated thymic lymphomas, n=4, p<0.005. IHC for PCNA in indicated thymic lymphomas (**n**). Quantification of the percentage of proliferation as assessed by PCNA staining (**o**), n=20 fields of 3 biological replicates, p<0.005. Statistical significance indicated by black asterisks.

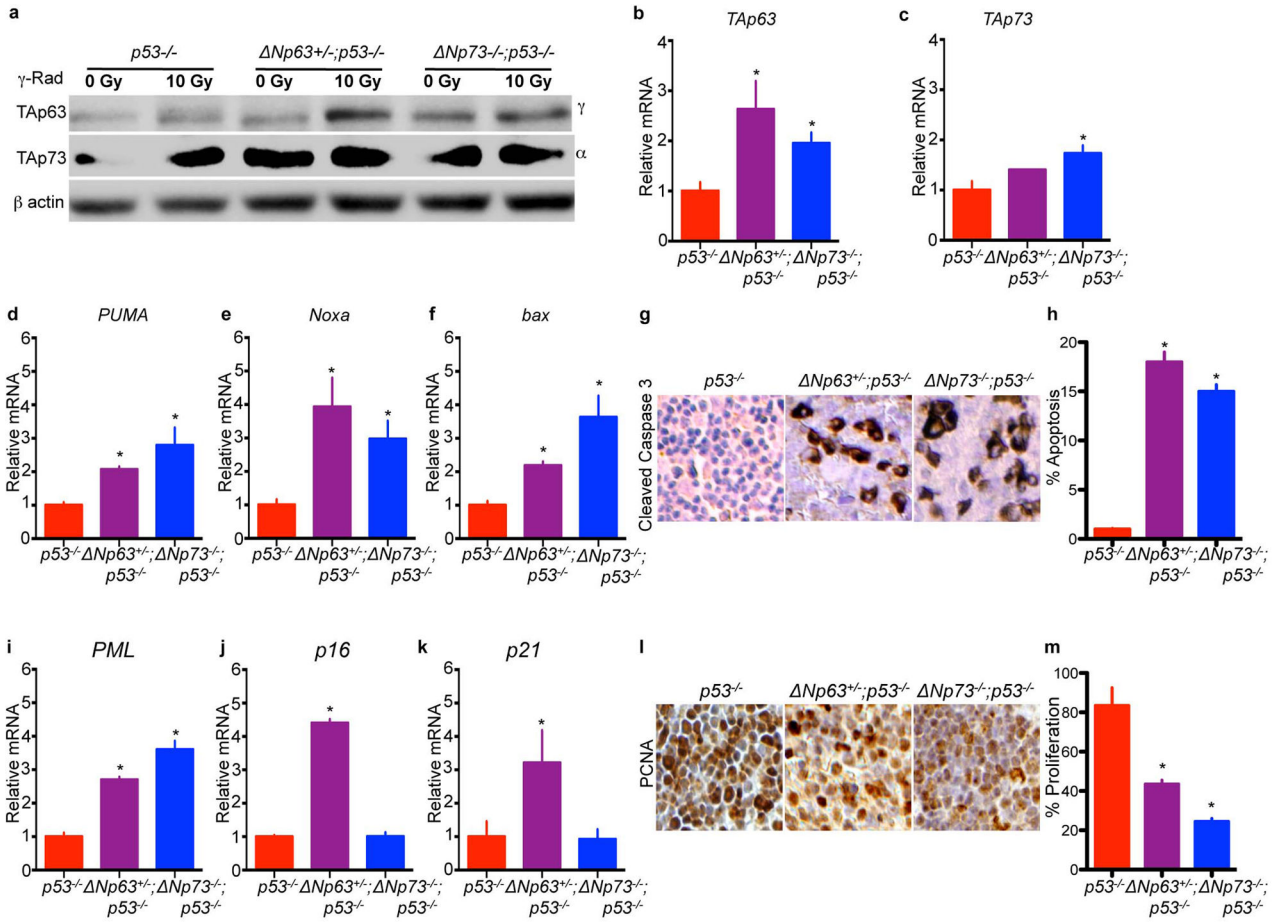

Extended Data Figure 3. Increased apoptosis and cell cycle arrest in Δ*Np63*+/−;*p53*−/− and Δ*Np73*−/−;*p53*−/− thymocytes after genotoxic stress

Western blot analysis in thymocytes derived from mice 6 hours after treatment with 0 Gy or 10 Gy gamma irradiation (**a**). Q-RT PCR for TAp63 (**b**), TAp73 (**c**), *PUMA* (**d**), *Noxa* (**e**), and *bax* (**f**) from samples shown in (a), n=4, p<0.005. Q-RT-PCR normalized to samples treated with 0 Gy. Immunohistochemistry (IHC) for cleaved caspase 3 in samples from (a) (**g**). Quantification of the percentage of apoptosis as assessed by cleaved caspase 3 staining

(**h**), n=20 fields of 3 biological replicates, p<0.005. Q-RT PCR for *PML* (**i**), *p16* (**j**), and *p21* (**k**) using total RNA from samples shown in (a), n=4, p<0.005. IHC for PCNA in samples shown in (a) (**l**). Quantification of the percentage of proliferation as assessed by PCNA staining (**m**), n=20 fields of 3 biological replicates, p<0.005. Statistical significance is indicated by black asterisks.

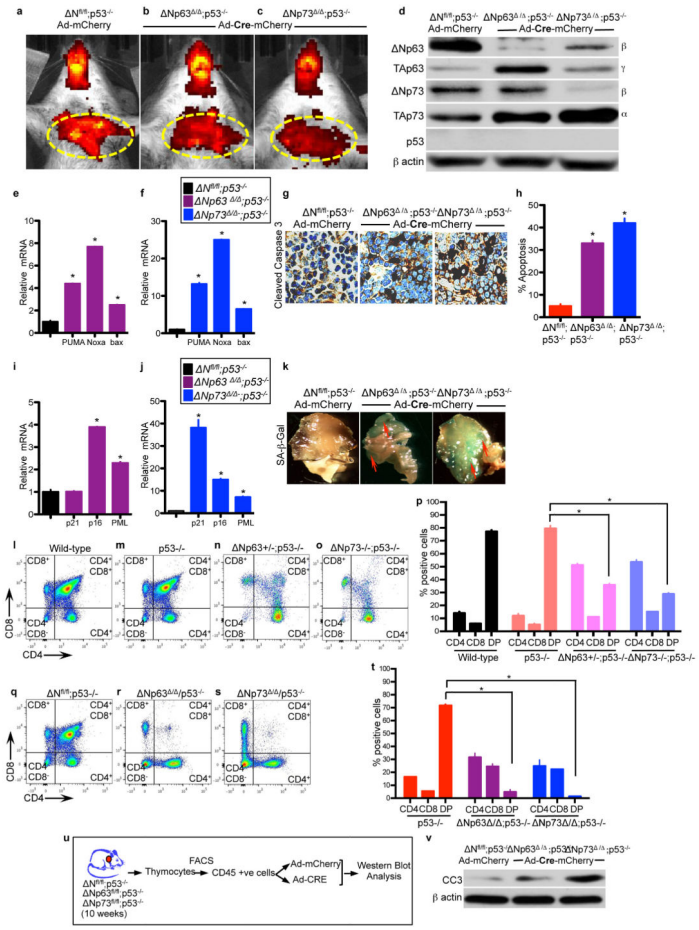

Extended Data Figure 4. *In vivo* intra-thymic delivery of Adenovirus-cre-mCherry

IVIS Lumina imaging of thymic lymphomas of mice of the indicated genotypes infected with Adenovirus (Ad)-mCherry (**a**) or Ad-Cre-mCherry (**b** & **c**) at 10 weeks of age and 48 hours after adenoviral delivery. Red fluorescence indicates viral delivery to the thymus shown by the yellow dashed ovals. Red fluorescence near the mouth is due to auto-fluorescence of calcium and mineral deposits in the teeth. Western blot analysis using lysates from indicated thymic lymphomas 48 hours after infection with Adenovirus (Ad)-mCherry or Ad-Cre-mCherry (**d**). Quantitative real time (qRT-PCR) of thymic lymphomas 48 hours after infection with Ad-mCherry (Δ*Nfl/fl;p53−/−*) or Ad-Cre-mCherry (Δ*Np63Δ/Δ;p53−/−* or Δ*Np73Δ/Δ;p53−/−*) (**e–f**). n=4, p<0.005. Immunohistochemistry (IHC) for cleaved caspase 3 in thymic lymphomas 48 hours after infection with Ad-mCherry (Δ*Nfl/fl;p53−/−*) or Ad-Cre-mCherry (Δ*Np63Δ/Δ;p53−/−* or Δ*Np73Δ/Δ;p53−/−*) (**g**). Quantification of apoptosis as assessed by cleaved caspase 3 staining of the indicated thymic

lymphomas (**h**), n=20 fields of 3 biological replicates, p<0.005. Q-RT-PCR of thymic lymphomas 48 hours after treatment with Ad-mCherry (Δ*Nfl/fl;p53*−/−) or Ad-Cre-mCherry (Δ*Np63*Δ/Δ*;p53*−/− or Δ*Np73*Δ/Δ*;p53*−/−), n=4, p<0.005 (**i–j**). Senescence associated beta galactosidase (SA-β-gal) staining (blue) of thymic lymphomas 48 hours after treatment with Ad-mCherry (Δ*Nfl/fl;p53*−/−) or Ad-Cre-mCherry (Δ*Np63*Δ/Δ*;p53*−/− or Δ*Np73*Δ/Δ*;p53*−/−) (**k**). Flow cytometry plots of the indicated thymocytes at 4-week of age **(l–o)**. Bar graph showing quantification of CD4, CD8, and CD4/CD8 double positive (DP) cells. n=3 mice per genotype, p<0.005 **(p)**. Flow Cytometry plots of thymic lymphoma cells 48 hours after adenovirus-mCherry or adenovirus-CRE treatment for the indicated genotypes (**q–s**). Bar graph showing quantification of CD4, CD8, and CD4/CD8 double positive (DP) cells in the indicated genotypes. n=3 mice per genotype, p<0.005 (**t**). Cartoon representation of isolation of CD45-postive thymic lymphoma cells from 10 week old mice of indicated genotypes **(u)**. Western blot analysis of CD45-postive thymic lymphoma cells after treatment with Ad-mCherry (ΔNfl/fl;p53−/−) or Ad-CRE-mCherry (ΔNp63Δ/Δ;p53−/− and ΔNp73Δ/Δ;p53−/−) (**v**). Statistical significance is indicated by black asterisks.

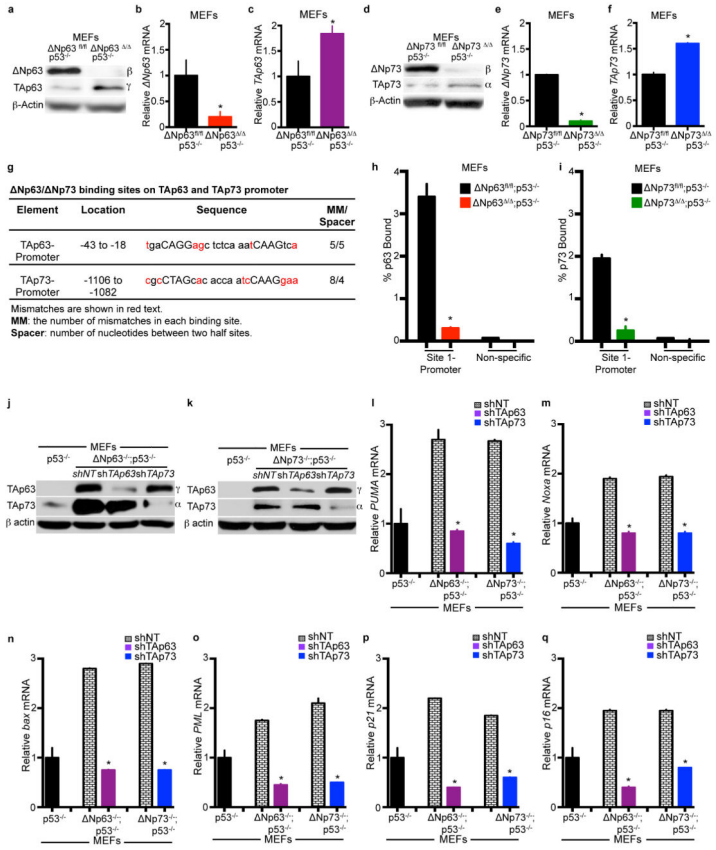

Extended Data Figure 5. Loss of ΔNp63/ΔNp73 induces TAp63 and TAp73 upregulation in the absence of *p53*.

Western blot analysis in Δ*Np63fl/fl;p53*−/− MEFs before (Δ*Np63fl/fl;p53*−/−) and after (Δ*Np63*Δ/Δ*;p53*−/−) Ad-cre administration **(a)**. Q-RT-PCR for ΔNp63 **(b)** and TAp63 **(c)** in indicated MEFs. Western blot analysis in Δ*Np73fl/fl;p53*−/− and Δ*Np73*Δ/Δ*;p53*−/− MEFs

(d). Q-RT-PCR for ΔNp73 **(e)** and TAp73 **(f)** in indicated MEFs. n=4, p<0.005. Table showing ΔNp63 and ΔNp73 binding sites on the TAp63 and TAp73 promoter regions **(g)**. Q-RT-PCR of chromatin Immunoprecipitation using indicated MEFs and an antibody for p63 **(h)** or p73 **(i)** n=3, p<0.005. Western blot analysis in Δ*Np63−/−;p53−/−* (**j**) or Δ*Np73−/−;p53−/−* (**k**) MEFs treated with the indicated shRNAs; (shNT) indicates a non-targeting scramble shRNA. Q-RT PCR for *PUMA* (**l**), *Noxa* (**m**), *bax* (**n**), *PML* (**o**), *p21* (**p**), and *p16* (**q**) in the indicated MEFs expressing the indicated shRNAs, n=5, p<0.005. Statistical significance indicated by black asterisks.

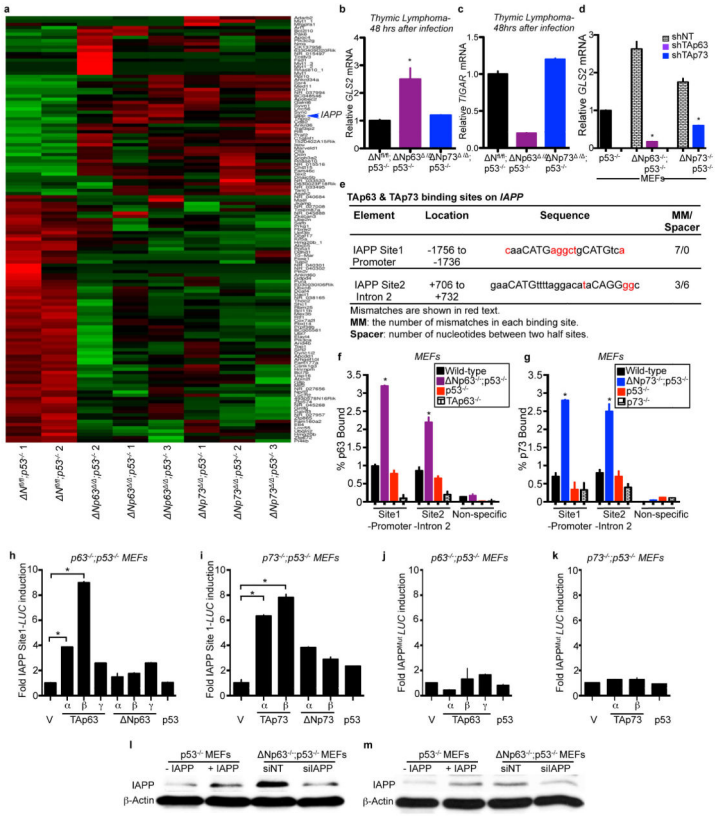

Extended Data Figure 6. Metabolic genes including *IAPP* are upregulated in thymic lymphomas deficient for ΔNp63 or ΔNp73 and p53

Supervised hierarchical clustering of RNA-sequencing data from thymic lymphomas 48 hours after treatment with Ad-mCherry (ΔNfl/fl;p53−/−) or Ad-Cre-mCherry (ΔNp63Δ/Δ;p53−/− or ΔNp73Δ/Δ;p53−/−) **(a)** Q-RT-PCR for *GLS2* (**b**) and *TIGAR* (**c**) in the indicated thymic lymphomas, n=4, p<0.005. Q-RT-PCR for *GLS2* in MEFs of the indicated genotypes expressing shRNAs for a non targeting sequence (shNT), *TAp63* (shTAp63) and *TAp73* (shTAp73) (**d**), n=4, p<0.005. Table showing the TAp63 and TAp73 binding sites on the *IAPP* promoter and intron 2 **(e)**. Q-RT-PCR of Promoter Site 1 using chromatin immunoprecipitation in MEFs (**f** & **g**) of the indicated genotypes, n=3, p<0.005. Dual luciferase reporter assay for pGL3-*IAPP*-Promoter Site 1 (**h** & **i**) and a mutant version of this reporter gene (pGL3-*IAPP* MUT) (**j** & **k**). Genotypes of MEFs and vectors used are shown. V represents pcDNA3 vector. Western blot analysis of the indicated MEFs

expressing IAPP or siRNAs for a non targeting sequence (siNT) or IAPP (siIAPP) (**l** & **m**). Statistical significance indicated by black asterisks.

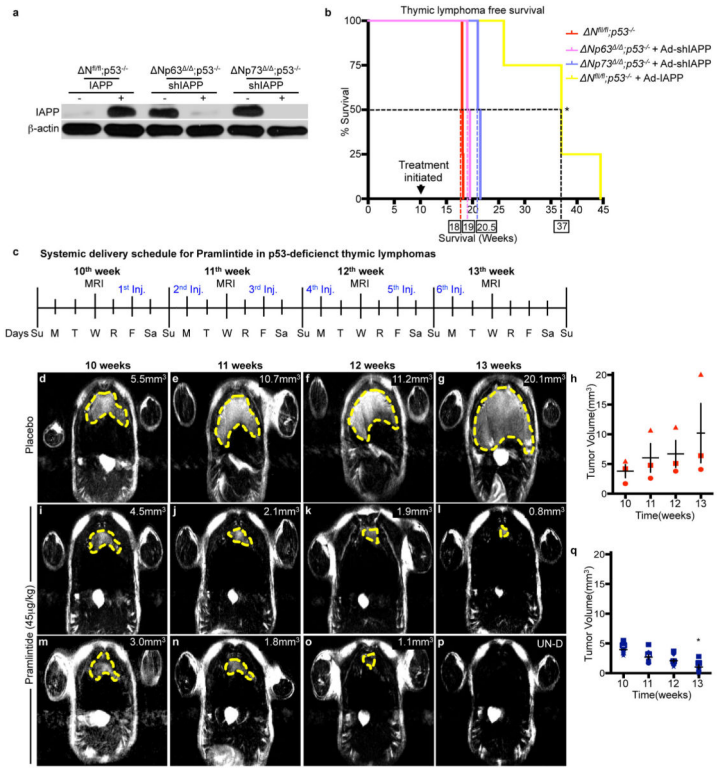

Extended Data Figure 7. Systemic *in vivo* delivery of pramlintide results in tumour regression in *p53* deficient thymic lymphomas

Western blot analysis showing IAPP expression in the indicated thymic lymphomas, n=5 mice (**a**). Kaplan Meier survival indicating thymic lymphoma free survival (**b**). n=8 mice per group, p<0.005. Cartoon indicating schedule of MRI imaging and injection (Inj.) of pramlintide in mice with *p53* deficient thymic lymphomas (**c**). MRI imaging at 10, 11, 12, and 13 weeks after treatment with placebo (**d–g**) or pramlintide (**i–p**). Quantification of tumour volumes in placebo (n=3) **(h)** and pramlintide treated mice (n=7) **(q)**, p<0.005. Statistical significance indicated by black asterisk.

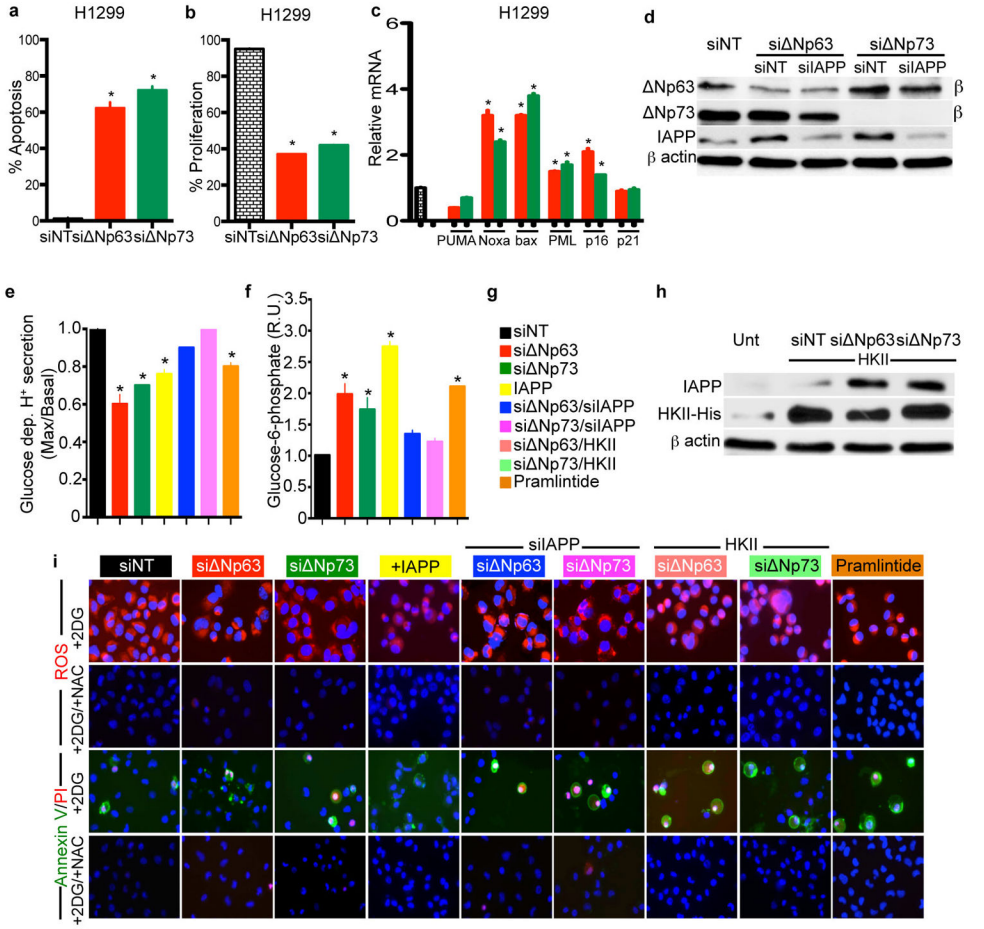

Extended Data Figure 8. IAPP inhibits glycolysis by increasing intra-cellular G-6-P levels

Quantification of apoptosis (**a**) and proliferation (**b**), n=20 fields of 3 biological replicates, p<0.005. Q-RT-PCR for the target genes indicated on the x-axis in the indicated H1299 cells expressing the indicated siRNAs (**c**), n=4. Asterisks indicate statistical significance (p<0.005) relative to siNT. Western blot analysis of H1299 cells treated with the indicated siRNAs (**d**). Bar graph indicating glucose dependent proton secretion as a measure of glucose uptake (**e**) and intracellular levels of glucose-6-phosphate in H1299 cells with the indicated siRNAs and treatments (**f**). Color coded legend for panels e, f & i (**g**). Western blot analysis of H1299 cells expressing the indicated siRNAs (**h**). Immunofluorescence analysis for ROS (red) or apoptosis (green or green/red) in H1299 cells expressing the indicated siRNAs and treated with 2DG and/or NAC (**i**).

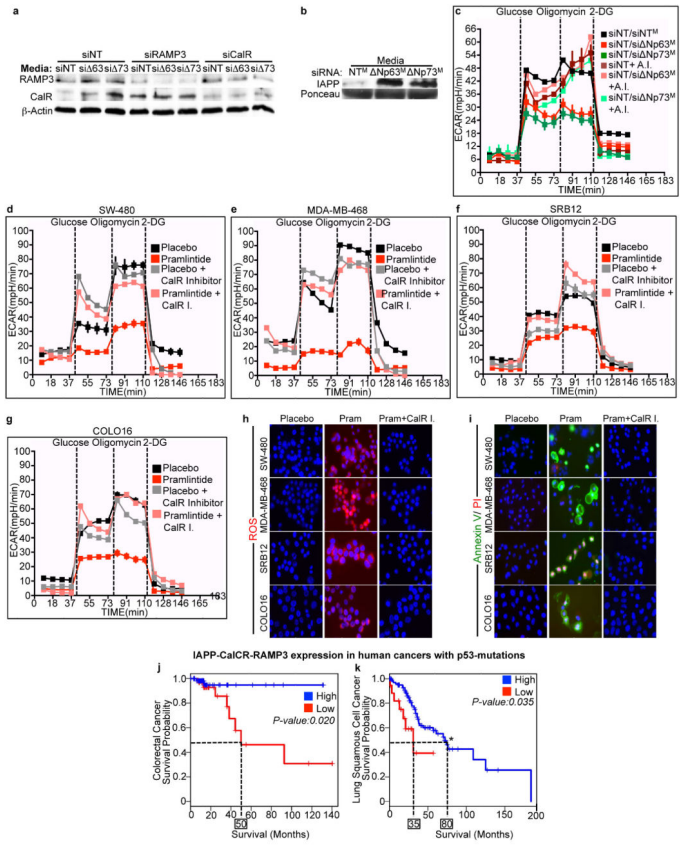

Extended Data Figure 9. Treatment of p53-mutant human cancer cell lines with pramlintide inhibits glycolysis and induces ROS and apoptosis

Western blot analysis of H1299 cells expressing the indicated siRNAs (**a)** or concentrated media derived from H1299 cells expressing siNT, siΔNp63, or siΔNp73 (**b**). Extracellular acidification rate (ECAR) using H1299 cells expressing the indicated siRNAs and treated with the indicated media containing secreted IAPP and treated with the indicated Amylin Inhibitor (A.I.) (**c**). Extracellular acidification rate (ECAR) as a measure of glycolysis in SW480 **(d)**, MDA- MB-468 **(e)**, SRB12 **(f)** and COLO16 **(g)** human cancer cell lines after treatment with placebo, pramlintide, or pramlintide and a calcitonin receptor inhibitor (CalR I.), n=3, p< 0.005. Glucose, oligomycin, and 2-Deoxy-D-Glucose (2-DG) were supplied to the media at the indicated time points shown on the x-axis. Immunofluorescence for ROS (red) **(h)** and apoptosis (green) **(i)** on the indicated cells, n=3. Kaplan Meier survival curves using data from patients with p53 mutant tumours with the indicated cancers and co-expression of IAPP, RAMP3 and CALCR (**j & k**). Boxed numbers represent median survival.

Acknowledgments

We thank A. Jain, V. Pant, J. Jackson, A. Marisetty, K. Michel and the Small Animal Imaging Facility (SAIF) for technical advice. This work was supported by grants to E.R.F. from NCI (R01CA160394) and (R01CA134796), CPRIT (RP120124), NCI- Cancer Center Core Grant (CA-16672)(University of Texas M.D. Anderson Cancer Center, a development award from the Lymphoma SPORE (P50CA136411), the Hildegardo E. and Olga M. Flores Foundation, and the Mel Klein Foundation and grant to J.B. from CPRIT (RP101243-P5). E.R.F. is a scholar of the

Leukemia and Lymphoma Society, the Rita Allen Foundation and the V Foundation for Cancer Research. A.V. is a Schissler Scholar and D.C. is a CPRIT Scholar (RP101502).

References

1. Ventura A, et al. Restoration of p53 function leads to tumour regression in vivo. Nature. 2007; 445:661–665.10.1038/nature05541 [PubMed: 17251932]
2. Wang Y, et al. Restoring expression of wild-type p53 suppresses tumor growth but does not cause tumor regression in mice with a p53 missense mutation. J Clin Invest. 2011; 121:893–904.10.1172/JCI44504 [PubMed: 21285512]
3. Flores ER, et al. Tumor predisposition in mice mutant for p63 and p73: evidence for broader tumor suppressor functions for the p53 family. Cancer Cell. 2005; 7:363–373. S1535-6108(05)00092-9 [pii]. 10.1016/j.ccr.2005.02.019 [PubMed: 15837625]
4. Su X, et al. TAp63 suppresses metastasis through coordinate regulation of Dicer and miRNAs. Nature. 2010; 467:986–990. nature09459 [pii]. 10.1038/nature09459 [PubMed: 20962848]
5. Su X, Chakravarti D, Flores ER. p63 steps into the limelight: crucial roles in the suppression of tumorigenesis and metastasis. Nat Rev Cancer. 2012; 13:136–143.10.1038/nrc3446 [PubMed: 23344544]
6. Tomasini R, et al. TAp73 knockout shows genomic instability with infertility and tumor suppressor functions. Genes Dev. 2008; 22:2677–2691. gad.1695308 [pii]. 10.1101/gad.1695308 [PubMed: 18805989]
7. Yang A, et al. p63, a p53 homolog at 3q27-29, encodes multiple products with transactivating, death-inducing, and dominant-negative activities. Mol Cell. 1998; 2:305–316. S1097-2765(00)80275-0 [pii]. [PubMed: 9774969]
8. Su X, et al. TAp63 is a master transcriptional regulator of lipid and glucose metabolism. Cell metabolism. 2012; 16:511–525.10.1016/j.cmet.2012.09.006 [PubMed: 23040072]
9. Flores ER, et al. p63 and p73 are required for p53-dependent apoptosis in response to DNA damage. Nature. 2002; 416:560–564. [pii]. 10.1038/416560a416560a [PubMed: 11932750]
10. Kenzelmann Broz D, et al. Global genomic profiling reveals an extensive p53-regulated autophagy program contributing to key p53 responses. Genes Dev. 2013; 27:1016–1031.10.1101/gad.212282.112 [PubMed: 23651856]
11. Di Como CJ, Gaiddon C, Prives C. p73 function is inhibited by tumor-derived p53 mutants in mammalian cells. Mol Cell Biol. 1999; 19:1438–1449. [PubMed: 9891077]
12. Gaiddon C, Lokshin M, Ahn J, Zhang T, Prives C. A subset of tumor-derived mutant forms of p53 down-regulate p63 and p73 through a direct interaction with the p53 core domain. Mol Cell Biol. 2001; 21:1874–1887.10.1128/MCB.21.5.1874-1887.2001 [PubMed: 11238924]
13. Lang GA, et al. Gain of function of a p53 hot spot mutation in a mouse model of Li-Fraumeni syndrome. Cell. 2004; 119:861–872. S0092867404010487 [pii]. 10.1016/j.cell.2004.11.006 [PubMed: 15607981]
14. Olive KP, et al. Mutant p53 gain of function in two mouse models of Li-Fraumeni syndrome. Cell. 2004; 119:847–860. S0092867404010463 [pii]. 10.1016/j.cell.2004.11.004 [PubMed: 15607980]
15. Chakravarti D, et al. Induced multipotency in adult keratinocytes through down-regulation of DeltaNp63 or DGCR8. Proc Natl Acad Sci U S A. 2014; 111:E572–581.10.1073/pnas.1319743111 [PubMed: 24449888]
16. Jacks T, et al. Tumor spectrum analysis in p53-mutant mice. Curr Biol. 1994; 4:1–7. [PubMed: 7922305]
17. Attardi LD, de Vries A, Jacks T. Activation of the p53-dependent G1 checkpoint response in mouse embryo fibroblasts depends on the specific DNA damage inducer. Oncogene. 2004; 23:973–980.10.1038/sj.onc.1207026 [PubMed: 14749764]
18. Bensaad K, et al. TIGAR, a p53-inducible regulator of glycolysis and apoptosis. Cell. 2006; 126:107–120. [PubMed: 16839880]
19. Li T, et al. Tumor suppression in the absence of p53-mediated cell-cycle arrest, apoptosis, and senescence. Cell. 2012; 149:1269–1283.10.1016/j.cell.2012.04.026 [PubMed: 22682249]

20. Suzuki S, et al. Phosphate-activated glutaminase (GLS2), a p53-inducible regulator of glutamine metabolism and reactive oxygen species. Proc Natl Acad Sci U S A. 2010; 107:7461–7466.10.1073/pnas.1002459107 [PubMed: 20351271]
21. Castle AL, Kuo CH, Han DH, Ivy JL. Amylin-mediated inhibition of insulin-stimulated glucose transport in skeletal muscle. Am J Physiol. 1998; 275:E531–536. [PubMed: 9725822]
22. Edelman S, Maier H, Wilhelm K. Pramlintide in the treatment of diabetes mellitus. BioDrugs. 2008; 22:375–386.10.2165/0063030-200822060-00004 [PubMed: 18998755]
23. Mattson MP, Goodman Y. Different amyloidogenic peptides share a similar mechanism of neurotoxicity involving reactive oxygen species and calcium. Brain Res. 1995; 676:219–224. [PubMed: 7796173]
24. Schubert D, et al. Amyloid peptides are toxic via a common oxidative mechanism. Proc Natl Acad Sci U S A. 1995; 92:1989–1993. [PubMed: 7892213]
25. Cairns RA, Harris IS, Mak TW. Regulation of cancer cell metabolism. Nat Rev Cancer. 2011; 11:85–95.10.1038/nrc2981 [PubMed: 21258394]
26. Pillay K, Govender P. Amylin uncovered: a review on the polypeptide responsible for type II diabetes. Biomed Res Int. 2013; 2013:826706.10.1155/2013/826706 [PubMed: 23607096]
27. Christopoulos G, et al. Multiple amylin receptors arise from receptor activity-modifying protein interaction with the calcitonin receptor gene product. Mol Pharmacol. 1999; 56:235–242. [PubMed: 10385705]
28. Masters SL, et al. Activation of the NLRP3 inflammasome by islet amyloid polypeptide provides a mechanism for enhanced IL-1beta in type 2 diabetes. Nat Immunol. 2010; 11:897–904.10.1038/ni.1935 [PubMed: 20835230]
29. Allen IC, et al. The NLRP3 inflammasome functions as a negative regulator of tumorigenesis during colitis-associated cancer. J Exp Med. 2010; 207:1045–1056.10.1084/jem.20100050 [PubMed: 20385749]
30. Vin H, et al. BRAF inhibitors suppress apoptosis through off-target inhibition of JNK signaling. Elife. 2013; 2:e00969.10.7554/eLife.00969 [PubMed: 24192036]
31. Liu P, Jenkins NA, Copeland NG. A highly efficient recombineering-based method for generating conditional knockout mutations. Genome Res. 2003; 13:476–484.10.1101/gr.749203 [PubMed: 12618378]
32. Lewandoski M, Wassarman KM, Martin GR. Zp3-cre, a transgenic mouse line for the activation or inactivation of loxP-flanked target genes specifically in the female germ line. Curr Biol. 1997; 7:148–151. [PubMed: 9016703]
33. Jackson JG, et al. p53-mediated senescence impairs the apoptotic response to chemotherapy and clinical outcome in breast cancer. Cancer Cell. 2012; 21:793–806.10.1016/j.ccr.2012.04.027 [PubMed: 22698404]
34. Su X, et al. TAp63 prevents premature aging by promoting adult stem cell maintenance. Cell Stem Cell. 2009; 5:64–75. [PubMed: 19570515]
35. Lin YL, et al. p63 and p73 transcriptionally regulate genes involved in DNA repair. PLoS Genet. 2009; 5:e1000680.10.1371/journal.pgen.1000680 [PubMed: 19816568]
36. Trapnell C, et al. Transcript assembly and quantification by RNA-Seq reveals unannotated transcripts and isoform switching during cell differentiation. Nat Biotechnol. 2010; 28:511–515.10.1038/nbt.1621 [PubMed: 20436464]
37. Huang da W, Sherman BT, Lempicki RA. Systematic and integrative analysis of large gene lists using DAVID bioinformatics resources. Nat Protoc. 2009; 4:44–57.10.1038/nprot.2008.211 [PubMed: 19131956]
38. Ardenkjaer-Larsen JH, et al. Increase in signal-to-noise ratio of > 10,000 times in liquid-state NMR. Proc Natl Acad Sci U S A. 2003; 100:10158–10163.10.1073/pnas.1733835100 [PubMed: 12930897]
39. Sandulache VC, et al. Glycolytic inhibition alters anaplastic thyroid carcinoma tumor metabolism and improves response to conventional chemotherapy and radiation. Mol Cancer Ther. 2012; 11:1373–1380.10.1158/1535-7163.MCT-12-0041 [PubMed: 22572813]
40. Maddocks OD, et al. Serine starvation induces stress and p53-dependent metabolic remodelling in cancer cells. Nature. 2013; 493:542–546.10.1038/nature11743 [PubMed: 23242140]

41. Comprehensive genomic characterization of squamous cell lung cancers. Nature. 2012; 489:519–525.10.1038/nature11404 [PubMed: 22960745]
42. Agrawal N, et al. Exome sequencing of head and neck squamous cell carcinoma reveals inactivating mutations in NOTCH1. Science. 2011; 333:1154–1157.10.1126/science.1206923 [PubMed: 21798897]
43. Stransky N, et al. The mutational landscape of head and neck squamous cell carcinoma. Science. 2011; 333:1157–1160. science.1208130 [pii]. 10.1126/science.1208130 [PubMed: 21798893]
44. Comprehensive molecular portraits of human breast tumours. Nature. 2012; 490:61–70.10.1038/nature11412 [PubMed: 23000897]
45. Banerji S, et al. Sequence analysis of mutations and translocations across breast cancer subtypes. Nature. 2012; 486:405–409.10.1038/nature11154 [PubMed: 22722202]
46. Comprehensive molecular characterization of human colon and rectal cancer. Nature. 2012; 487:330–337.10.1038/nature11252 [PubMed: 22810696]
47. Cerami E, et al. The cBio cancer genomics portal: an open platform for exploring multidimensional cancer genomics data. Cancer discovery. 2012; 2:401–404.10.1158/2159-8290.CD-12-0095 [PubMed: 22588877]

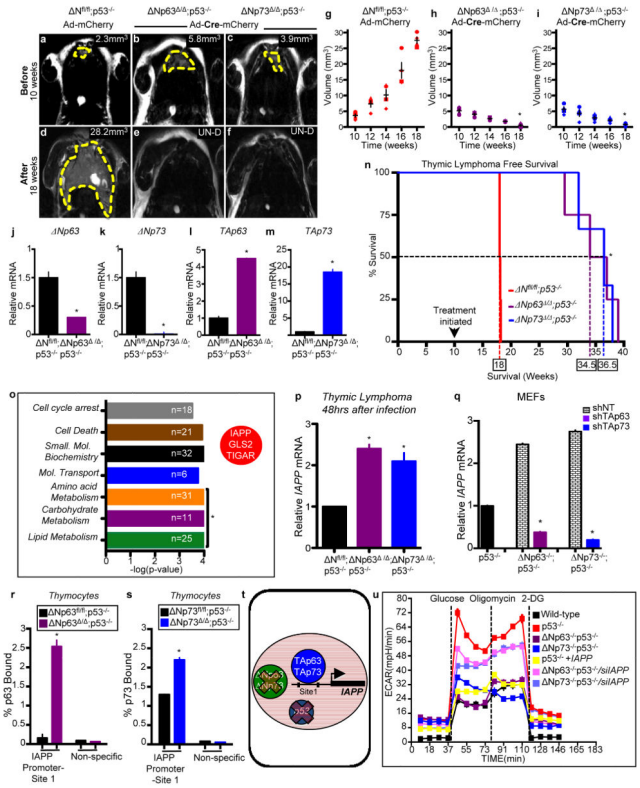

Figure 1. *In vivo* deletion of Δ*Np63* or Δ*Np73* in p53-deficient mice suppresses lymphomagenesis

Magnetic Resonance Imaging (MRI) of thymic lymphomas of indicated mice (**a–f**). Tumour volume (mm^3) within each panel. UN-D = undetectable. Tumours indicated by the dashed yellow line. Quantification of the indicated thymic lymphomas (**g–i**), n=9 mice. Quantitative real time (qRT-PCR) (**j–m**). n=4, p<0.005. Kaplan Meier curve (**n**), n=9, p<0.005. Boxed numbers represent median survival. Ingenuity Pathway Analysis (IPA) of RNA-sequencing from thymic lymphomas 48 hours after infection with adenoviruses (**o**). Red oval indicates significantly upregulated metabolic genes. Q-RT-PCR for *IAPP* in thymic lymphomas (**p**) or MEFs of the indicated genotypes using a non-targeting shRNA (shNT) or shRNAs for TAp63 (shTAp63) or TAp73 (shTAp73) (**q**), n=4, p<0.005. Q-RT-PCR of IAPP Promoter Site 1 using chromatin immunoprecipitation (**r** & **s**), n=3, p<0.005. Cartoon showing transcriptional activation of *IAPP* by TAp63 and TAp73 (**t**). Extracellular acidification rate (ECAR) as a measurement of glycolysis (**u**), p<0.005.

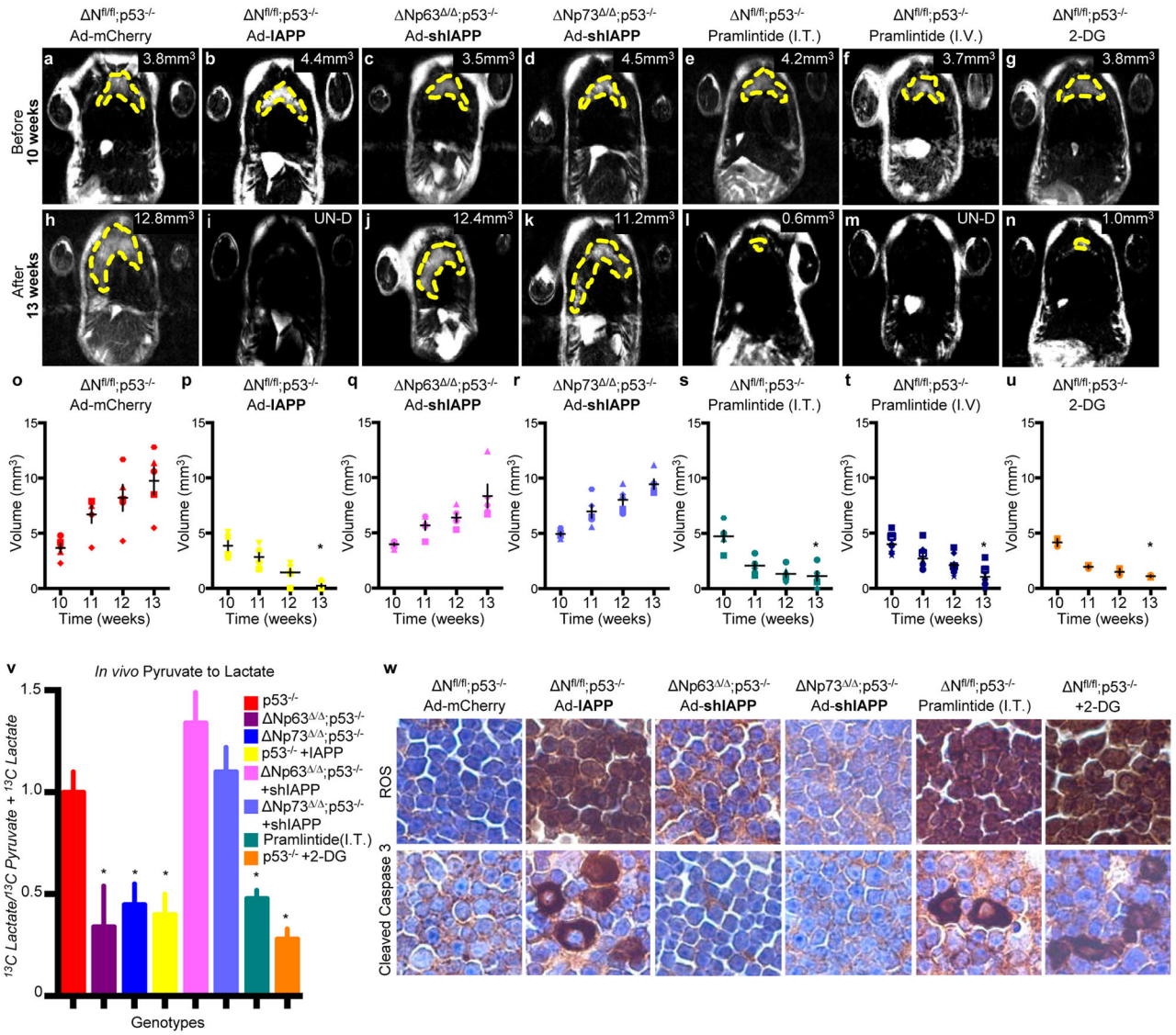

Figure 2. IAPP is causally involved to suppress tumourigenesis in *p53* deficient thymic lymphomas

Thymic lymphomas were infected with Adenovirus (Ad)-mCherry (**a & h**), Adenovirus (Ad)-IAPP-mCherry (+IAPP)(**b & i**), Ad-shIAPP-mCherry (**c, d, j & k**), or treated with pramlintide intratumoural (I.T.) (**e & l**) or intraveneous (I.V.) (**f & m**), or 2-DG (**g & n).** Yellow dashed lines indicate tumour. Volume of tumour shown. UN-D = undetectable. Quantification of the indicated thymic lymphomas (**o–u**). n=7 mice per group. Significance indicated by the asterisks, p<0.005. Quantification of *in vivo* pyruvate to lactate conversion using dynamic magnetic resonance spectroscopy as a measurement of glycolysis, n=3 mice, p<0.005 (**v**). Immunohistochemistry for reactive oxygen species (ROS) or cleaved caspase 3 (**w**). Positive nuclei are brown.

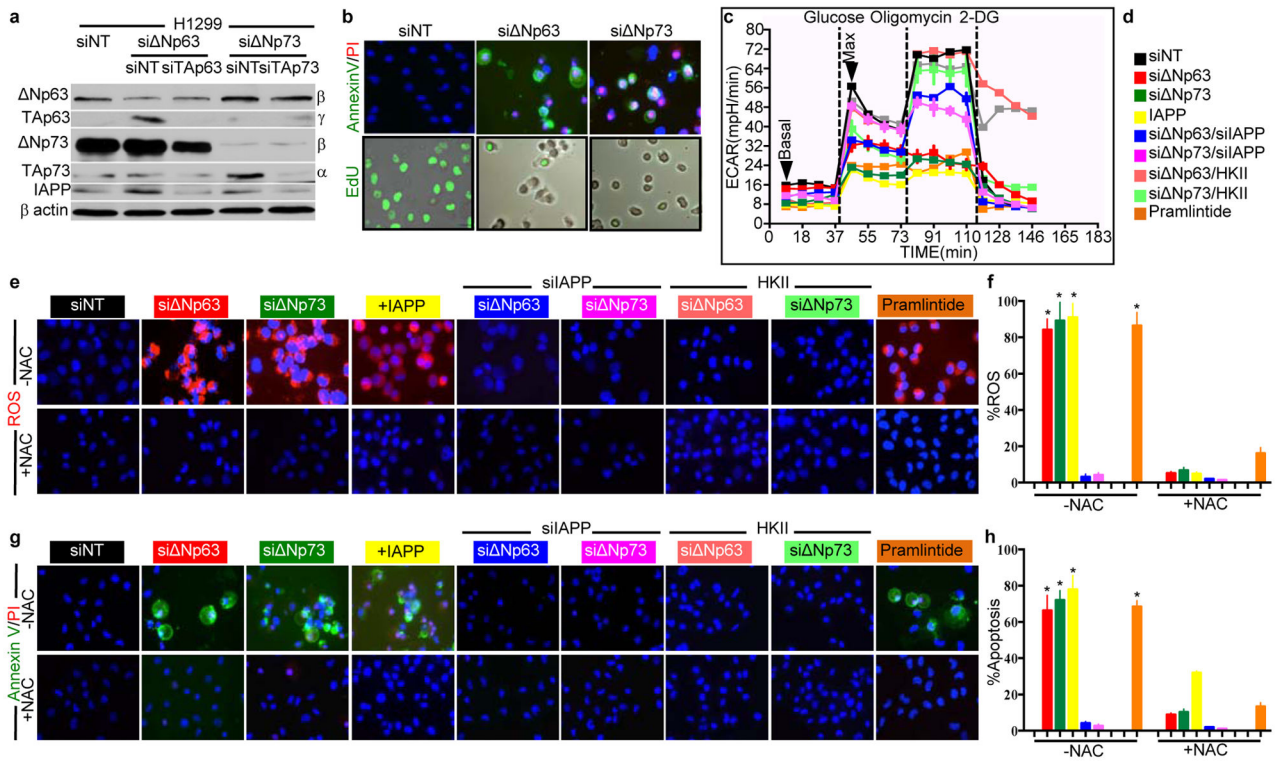

Figure 3. IAPP inhibits glycolysis and induces ROS and apoptosis in p53 deficient human cancer cell lines

Representative western blot analysis (**a**), n=4. Immunofluorescence (IF) for apoptosis and EdU incorporation (**b**). Extracellular acidification rate as a measure of glycolysis (**c**), n=3, p<0.005. Legend in **d** is color-coded and corresponds to panels **c, e–h**. Immunofluorescence (IF) (**e**) and quantification (**g**) for ROS (red) or apoptosis (green or green/red) (**g & h**).

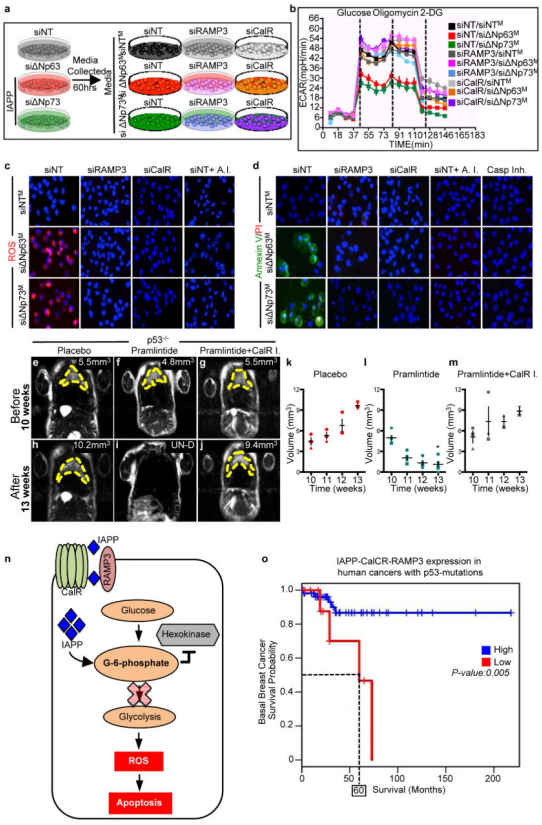

Figure 4. Calcitonin and RAMP3 receptors are required for secreted IAPP to suppress tumorigenesis

Cartoon depicting treatment of cells expressing the indicated siRNAs and treated with media from the cells secreting IAPP on the left (**a**). Extracellular acidification rate (ECAR) in H1299 cells (**b**). Immunofluorescence (IF) for ROS (**c**) and apoptosis (**d**). MRI and quantification of thymic lymphomas treated with placebo (**e, h, & k**), pramlintide (**f, i, & l**), or pramlintide plus calcitonin inhibitor (CalR I) (**g, j, & m**), n=5 mice. Cartoon of IAPP signaling through RAMP3 and calcitonin receptor (CALCR) to inhibit glycolysis and induce ROS and apoptosis (**n**). Kaplan Meier curves from patients with p53 mutant tumours and co-expression of IAPP, RAMP3 and CALCR (**o**). Boxed numbers represent median survival.